Title
Dynamics of information processing in the hippocampal network

Author
Carr, Margaret F.

Publication Date
2011

Peer reviewed|Thesis/dissertation

Dynamics of information processing in the hippocampal network

by

Margaret F. Carr

DISSERTATION

Submitted in partial satisfaction of the requirements for the degree of

DOCTOR OF PHILOSOPHY

in

Neuroscience

in the

GRADUATE DIVISION

of the

UNIVERSITY OF CALIFORNIA, SAN FRANCISCO

Acknowledgements

I would like to thank Paul Larkin for his love and encouragement, my family for their advice and perspective, and my classmates for their friendship and support. I would like to acknowledge members of the Frank Lab—especially Sen Cheng, Surya Ganguli, Sheri Harris, Mattias Karlsson, Caleb Kemere, Steve Kim, Christy Lykken, Ana Nathe, and Annabelle Singer—for all that they have taught me and my rotation students—Jason Chung , Patricia Correia, Lynne Tye, Kate Vitale, and Jeanette Wickelgren—for teaching me how to be a mentor. My thesis committee—Patricia Janak, Michael Brainard, and Flip Sabes—always asked insightful questions and gave great advice. Most of all, I thank Loren Frank, who is an outstanding mentor, scientist, and teacher. This work was supported by a National Science Foundation Graduate Research Fellowship and NIH grant F31MH093067.

Portions of the introduction have been published as a review article in Nature Neuroscience, the coauthors listed in this publication helped write and edit the manuscript. Chapter 1 is the work of Margaret Carr with contributions from Mattias Karlsson, who performed the recordings, and Loren Frank who directed and supervised the research. Chapter 2 is the work of Margaret Carr with contributions from Caleb Kemere, who helped collect and analyze the electrical stimulation data, Mattias Karlsson, who performed some of the recordings, and Loren Frank, who directed and supervised the research.

Dynamics of information processing in the hippocampal network.

Margaret F. Carr

We rely on our memories of past experiences, in conjunction with our current perception of the external world, to guide our behavior. The hippocampus is essential for rapidly encoding new memories. Subsequent processes between the hippocampus and distributed neocortical circuits are thought to consolidate these memories for long term storage and to retrieve stored memories to guide ongoing behavior. These varied mnemonic functions are thought to be subserved by distinct patterns of activity in the hippocampal subfields. In particular, the highly recurrent hippocampal area CA3 is crucial for the formation and consolidation of stored associations. As the associations formed in the recurrent CA3 network can only influence the neocortex via hippocampal output area CA1, understanding when how and when CA3 communicates with CA1 is critical for understanding memory processes. In Chapter 1 we investigate how CA3 and CA1 are coordinated during sharp wave-ripple events (SWRs) that are thought to support memory consolidation. We find that during SWRs there is a transient increase in the gamma synchrony between CA3 and CA1 and that the degree of synchronization between CA3 and CA1 is predictive of the quality of the replay of past experiences. Our results suggest that transient CA3-CA1 gamma synchronization is a central component of SWRs and this synchronization serves to clock the reactivation of stored memories across the hippocampal network. In Chapter 2 we investigate how the influence of CA3 on CA1 varies as a function of ongoing behavior. We find that as animals move faster, the influence of CA3 on CA1 decreases and that the level of coordinated spiking activity in CA1 reflects the influence of CA3. Our results suggest that movement speed drives a dynamic balance between learned associations and more independent sensory representations in the hippocampus which appears well suited to support the multiple mnemonic functions of the hippocampal circuit.

Table of contents

List of figures

Introduction

Chapter 1 | Transient gamma synchrony underlies hippocampal memory replay

Chapter 2 | Continuous network states in the hippocampus

Introduction

Our memories are central to our sense of self. We use past experiences to guide current decisions, an ability that requires both memory storage and retrieval. The highly plastic hippocampal circuit is believed to be the initial site of encoding episodic memories. Studies of hippocampal lesions have suggested that there is a subsequent process during which the hippocampus interacts with the rest of the brain to engrain stable, long lasting representations in hippocampal-neocortical circuits (Squire and Zola-Morgan, 1991, Kim and Fanselow, 1992, Dudai, 2004). While there is still debate about how long this consolidation process lasts and whether memories ever become truly independent of the hippocampus (Jarrard, 2001, Nadel and Moscovitch, 2001), it is clear that the hippocampus plays an essential role in the initial encoding and subsequent stabilization of long term memories (Squire, 1982, Cohen and Eichenbaum, 1993, Rudy and Sutherland, 1995). This stabilization is thought to depend on the reactivation of previously encoded associations, engraining those associations into the less-plastic neocortex (Alvarez and Squire, 1994, Eichenbaum and Cohen, 2001).

In the freely moving animal, pyramidal neurons in the hippocampus show firing responses that are tuned to specific locations in space such that in a given environment, neurons are active when the animal visits a particular limited region, and is nearly silent elsewhere (O'Keefe and Dostrovsky, 1971, O'Keefe and Nadel, 1978). The receptive fields of these “place cells” develop with experience, indicating that place cells “learn” to encode spatial information in a context dependent manner (Wilson and McNaughton, 1993, Frank et al., 2004). Behavioral trajectories from one location to another in space are thus represented by the hippocampus as a sequence of place cells.

During sharp wave ripples (SWRs), these sequences of place cells representing previously experienced behavioral trajectories are replayed on a compressed timescale,

suggesting a role for reactivation in consolidation (Buzsaki, 1986, Wilson and McNaughton, 1994, Eichenbaum and Cohen, 2001, Nakashiba et al., 2009, Diekelmann and Born, 2010). SWR replay can occur in either the same (forward) or the opposite (reverse) direction as observed during behavioral traversal (Foster and Wilson, 2006, Diba and Buzsaki, 2007) (Figure 1) and the direction of replay is related to the animal's behavior. Reverse replay occurs preferentially at the end of runs when the animal reached the reward location, potentially linking behavioral trajectories to their outcomes (Foster and Wilson, 2006). Forward replay occurs preferentially at the beginning of runs, perhaps providing information relevant for evaluating future trajectories (Diba and Buzsaki, 2007). Behaviorally relevant sequences are replayed repeatedly during SWRs, such that sequences can be replayed more often than the trajectories they represented had been experienced (Foster and Wilson, 2006). SWR replay is seen immediately after the very first traversal; demonstrating that the hippocampus can replay sequences that are experienced only once and suggesting that replay contributes to one-trial learning.

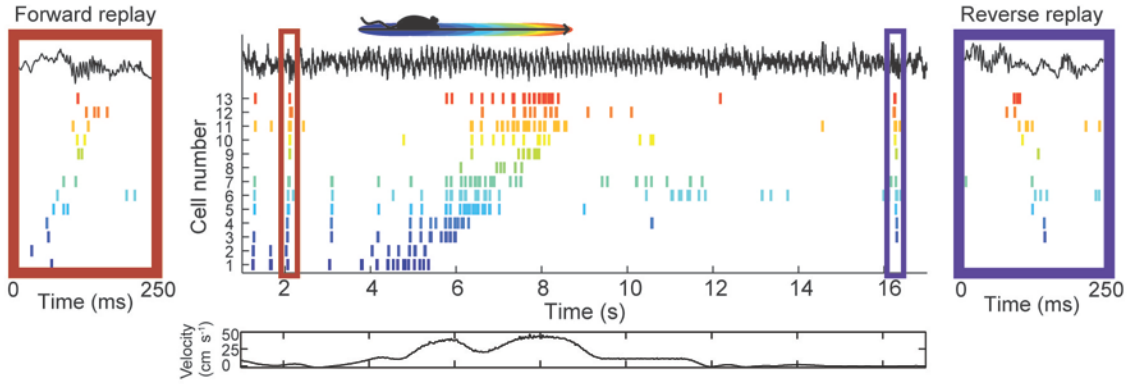

Figure 1 | Place cell sequences experienced during behavior are replayed in both the forward and reverse direction during SWRs. Spike trains for 13 neurons with place fields on the track are shown before, during, and after a single traversal of a linear track. Sequences that occur during running (center) are reactivated during SWRs. Forward replay (left inset, red box) occurs before traversal of the envrionment and reverse replay (right inset, blue box) afterwards. The CA1 local field potential is shown on top and the animal's velocity is shown below. Adapted from Diba and Buzsaki, 2007.

Sharp-wave ripples originate in the hippocampus and are triggered by synchronized activation of CA3 pyramidal cells, leading to characteristic negative potentials (sharp waves) in the CA1 stratum radiatum (Buzsaki, 1986, Ylinen et al., 1995, Csicsvari et al., 2000, Sullivan et al., 2011) (Figure 2). When recording in area CA3, this synchronized activation of local pyramidal cells can be measured as a 100-150 Hz oscillation (Csicsvari et al., 1999). The population burst in the CA3 region recruits CA1 pyramidal cells as well as basket and chandelier cells, leading to a transient (~100 ms) “ripple” oscillation (150-250Hz) in the CA1 pyramidal cell layer (Ylinen et al., 1995). The short latency bursts of CA3 and CA1 neurons during SWRs appear well suited to induce synaptic plasticity (Buzsaki, 1986, 1989). SWRs are prominent during sleep as well as in the awake state during immobility, consummatory behavior, grooming (Buzsaki et al., 1983, Buzsaki, 1986), and can also be seen during running (O'Neill et al., 2006, Cheng and Frank, 2008). Activity during SWRs propagates from CA3 to CA1, one of the major output areas of the hippocampus, and then out to neocortex (Chrobak and Buzsaki, 1996, Siapas and Wilson, 1998, Wierzynski et al., 2009).

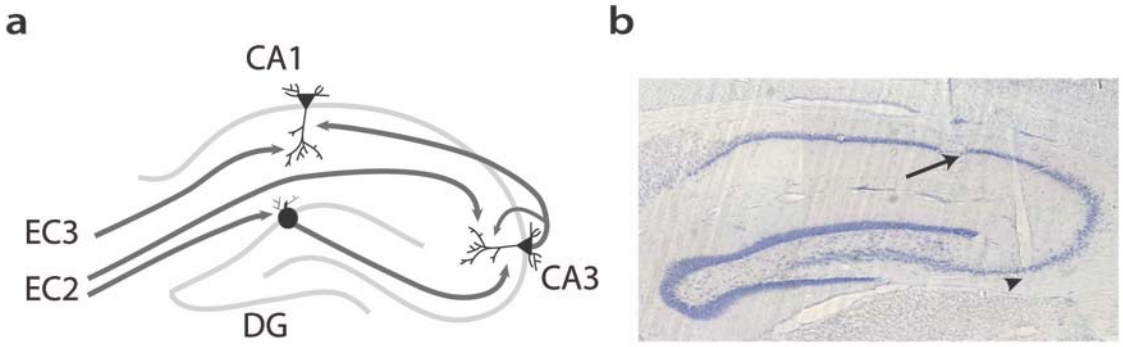

Figure 2 | Hippocampal anatomy. **(a)** The hippocampus consists of multip distinct subregions: the detate gyrus (DG), the highly recurrent CA3, and output region CA1. Arrows indicate excitatory connections. Information about the external world reaches the hippocampus via the superficial layers of the entorhinal cortex (EC). **(b)** Histology showing recording locations in CA3 (arrowhead) and CA1 (arrow).

The extensive excitatory recurrent connections among CA3 pyramidal cells (Amaral et al., 1990) have led some to suggest that CA3 acts as an auto-associative pattern completion network (Marr, 1971, McNaughton and Morris, 1987). Thus the activation of a small subset of CA3 neurons could initiate a cascade of excitation across previously modified synapses, leading to reverberating activity that eventually settles into an attractor state corresponding to a previously stored memory. Reinstatement of stored representations in CA3 could then reinstate the corresponding representations in CA1 through feed forward excitation. Hippocampal replay during SWRs is thought to reflect this type of auto-associative pattern completion in CA3 in conjunction with feed forward recruitment of pyramidal cells and interneurons in CA1. This model is consistent with the observation that the fidelity of reactivation (measured across cell pairs) is higher in CA3 than CA1 (Karlsson and Frank, 2009). Furthermore, CA3 output is necessary for SWR reactivation of CA1 representations (Nakashiba et al., 2009).

For both chapters presented in this thesis, we investigate how CA3 communicates with CA1. In the first chapter we asked how spatially distributed populations of CA3 and CA1 neurons can become coordinated during SWRs to replay learned associations with high fidelity. We show that during SWRs there are transient increases in gamma (20-50Hz) power and synchrony across the dorsal CA3 and CA1 networks. These gamma oscillations entrain CA3 and CA1 spiking. Moreover, during awake SWRs higher levels of gamma synchrony are predictive of higher quality replay of past experiences. These results indicate that CA3-CA1 gamma synchronization is a central component of awake memory replay and suggest that transient gamma synchronization serves as a clocking mechanism to enable consistent memory reactivation across the hippocampal network.

In the second chapter we asked how the influence of CA3 on CA1 varies as a function of ongoing behavior. Standard models of hippocampal function have posited two

distinct processing states: encoding of memories driven by sensory input from the entorhinal cortex and subsequent consolidation of those memories driven by the recurrent CA3 network (Buzsaki, 1989). We show that rather than a two state model, ongoing behavior continuously modulates the influence of internal representations from CA3 on activity in CA1. We show that as animals move faster, the influence of CA3 on CA1 decreases as measured by the amplitude of SWRs, the power of slow gamma oscillations, and the synaptic strength of the CA3-CA1 pathway. The level of coordinated spiking activity in CA1 reflects the influence of CA3: cell assemblies are highly correlated at low speeds and become progressively less correlated with increasing movement speed. These results suggest that movement speed drives a dynamic balance between learned associations and more independent sensory representations in the hippocampus which appears well suited to support the multiple mnemonic functions of the hippocampal circuit.

Chapter 1

Transient gamma synchrony underlies hippocampal memory replay

Abstract

The replay of previously stored memories during hippocampal sharp wave ripples (SWRs) is thought to support their consolidation in distributed hippocampal-neocortical networks. These replay events consist of precisely timed sequences of CA3 and CA1 neural activity that are coordinated within and across hemispheres. The mechanism of this coordination is not understood. Here we show that during SWRs recorded in both awake and quiescent states there are transient increases in gamma (20-50 Hz) power and synchrony across the dorsal CA3 and CA1 networks of both hemispheres. These gamma oscillations entrain CA3 and CA1 spiking. Moreover, during awake SWRs higher levels of gamma synchrony are predictive of higher quality replay of past experiences. Our results indicate that CA3 – CA1 gamma synchronization is a central component of awake memory replay and suggest that transient gamma synchronization serves as a clocking mechanism to enable consistent memory reactivation across the hippocampal network.

Introduction

The hippocampus is essential for encoding and consolidating memories of experiences (Cohen and Eichenbaum, 1993). During exploration of an environment, subsets of CA3 and CA1 neurons are active in one or more restricted regions, the neurons “place field” (O'Keefe and Dostrovsky, 1971, O'Keefe and Nadel, 1978). This internal representation of the external world develops as animals learn about new

locations (Wilson and McNaughton, 1993, Frank et al., 2004). These learned representations are replayed during sharp-wave ripple (SWR) events that occur during periods of awake stillness and slow wave sleep (Wilson and McNaughton, 1994, Lee and Wilson, 2002, Foster and Wilson, 2006, Karlsson and Frank, 2009). Disruption of SWRs during sleep following learning impairs subsequent performance (Girardeau et al., 2009, Ego-Stengel and Wilson, 2010), suggesting that hippocampal reactivation plays an important role in memory consolidation.

The SWRs in which memory reactivation occurs are transient population events that originate in hippocampal area CA3. Near synchronous activation of neurons in CA3 is associated with the characteristic sharp-wave recorded in CA1 stratum radiatum and results in recruitment of excitatory and inhibitory neurons in CA1, generating the fast ripple oscillation (150-250Hz) in stratum pyramidale (Buzsaki, 1986, Buzsaki et al., 1992, Ylinen et al., 1995, Csicsvari et al., 2000). During SWRs, excitatory neurons in both CA3 and CA1 fire in short-latency bursts and CA1 neurons are phase-locked to the local ripple oscillations (Buzsaki et al., 1992, Ylinen et al., 1995, Csicsvari et al., 2000). Notably, SWRs often occur concurrently across hemispheres (Ylinen et al., 1995). While SWRs occur concurrently, the high frequency ripple oscillations are not coherent between CA3 and CA1 (Csicsvari et al., 1999) or across hemispheres (Ylinen et al., 1995), suggesting that the ripple oscillation itself is an unlikely mechanism to coordinate memory replay events across the spatially distributed hippocampal network.

We investigated possible mechanisms that could support the dynamic formation of CA3 and CA1 cell assemblies that replay representations of previous experience during SWRs. We show that replay events involve precisely timed activation of neurons from both hemispheres and find that there are specific patterns of gamma synchrony between CA3 and CA1 that are present during SWRs. This transient gamma synchronization entrains spiking across regions and hemispheres, suggesting that the

gamma rhythm serves as a clocking mechanism to enable consistent sequential reactivation across the hippocampal network.

Results

Bilateral dorsal CA3 and CA1 stratum pyramidale recordings were obtained from three rats as they performed a hippocampally-dependent spatial alternation task (Kim and Frank, 2009) in two initially novel W-shaped environments and during interleaved rest sessions in a high-walled enclosure (Karlsson and Frank, 2008, 2009) (Figure 1a). Each rat was exposed to a single W-track for two run sessions per day for either 6 (rats 1 and 2) or 3 (rat 3) consecutive days before the first exposure to the second W-track (Figure S1). SWRs were detected by selecting periods when ripple power (150-250Hz) on any tetrode targeting CA1 stratum pyramidale exceeded 3 standard deviations above the mean when animals were moving less than 4 cm/second. All findings were consistent across individual animals.

Large populations of spatially distributed neurons frequently reactivate previous experiences during SWRs. As illustrated in this example, neurons recorded bilaterally from both CA3 and CA1 are interleaved throughout each SWR (Figure 1b). We used a Bayesian decoder with a uniform prior to translate the ensemble spiking of this event into probability distributions over positions using place fields recorded in a previously experienced environment (Davidson et al., 2009, Karlsson and Frank, 2009) (see Methods). In this example, the neurons that fired earliest in time had place fields nearest the center well, whereas neurons that had place fields further from the center well fired progressively later in time (Figure 1c). Over the course of this SWR, a previously experienced behavioral trajectory (from center to outside reward well) was reactivated. This decoded sequence of positions corresponded to a coherent spatial trajectory that was very unlikely to occur by chance ($p < 10^{-5}$).

We consistently observed the participation of neurons from spatially distributed networks during SWRs. Combining across all run and rest sessions, ninety-eight percent (655 out of 667) of significant replay events had neurons from both CA1 and CA3 participating, and 89% (589 out of 667) of significant replay events had participating neurons from both hemispheres. Reactivation depends on the integrity of the CA3-CA1 network (Nakashiba et al., 2009) and reflects activity generated in the hippocampus (Chrobak and Buzsaki, 1994, 1996, Sullivan et al., 2011), suggesting that a spatially coherent network pattern coordinates activity across CA3 and CA1 bilaterally during SWRs (Figure 1d). We therefore examined the structure of network activity in CA3 and CA1 during SWRs. We and others have shown that spiking during SWRs differs depending on whether the animal is awake or in a quiescent, sleep-like state (O'Neill et al., 2006, Karlsson and Frank, 2009, Dupret et al., 2010a), so we examined awake and quiescent SWRs separately.

LFP activity during awake SWRs

We asked what patterns of local field potential (LFP) activity are present during SWRs. We found that in both CA3 and CA1 there was a transient increase in gamma power (20-50Hz) concurrent with the increased power in the ripple band (Figure 2a-b; data from an example run session). To measure changes in gamma power, we computed a spectrogram around the time of each SWR (-400 ms to 400 ms from the time of SWR detection) for each tetrode located in CA3 or CA1 stratum pyramidale using the multi-taper method (Percival and Walden, 1993, Bokil et al., 2010) (see Methods). For this and all other spectral analyses we used 100 ms non-overlapping bins. We then converted the power in each frequency band to a z-score and averaged the spectrograms across tetrodes for each region. Multiple SWRs can occur in trains with close temporal proximity (Davidson et al., 2009), so we restricted our analysis to the first

SWR of each train (see Methods). We found that gamma power in both CA1 and CA3 increased substantially above baseline levels at the time of SWR detection, reached peak amplitude at the peak of the SWR, remained elevated throughout the SWR and began to decay towards baseline values after 200 ms (Figure 2c-d; Kruskal-Wallis ANOVA, post-hoc tests; n = 7653 SWRs from 74 behavioral sessions; gamma power > baseline; CA1: 0ms-400ms, peak, $p<10^{-5}$, CA3:0-300ms, peak $p<10^{-5}$; 400ms $p<0.05$; for all analyses baseline was defined as the average value occurring -450 to -400 ms before SWR detection). As the duration of SWRs can vary from tens to hundreds of milliseconds and SWRs can occur in trains, the average gamma power can remain elevated for a period of time after the initial SWR detection before returning to baseline levels (not shown). The significant transient increase in CA3 and CA1 gamma power during SWRs was visible in the raw LFP trace (Figure 2e, example trace, same SWR as shown in Figure 1a-c).

As expected, we also observed an increase in power for frequencies less than 20Hz in CA1 corresponding to the sharp-wave (Buzsaki, 1986). We also observed a small but significant increase in fast gamma power (60-100Hz; Figure S2). We focused on the transient increase in slow gamma (20-50Hz) power because it was significantly larger than the increase in fast gamma power (Kruskal-Wallis ANOVA, post-hoc tests; slow gamma power > fast gamma power, $p<0.05$) and because slow gamma oscillations in CA1 are thought to reflect coupling between CA1 and CA3 (Bragin et al., 1995, Colgin et al., 2009).

If oscillations in the gamma band are characteristic of SWRs, then the amplitude of gamma and ripple oscillations should be related. Therefore we asked whether this transient increase in gamma power during SWRs co-varied with ripple power. We found that gamma power in both CA1 and CA3 was correlated with ripple power on a SWR by SWR basis, with the correlation significantly greater than baseline for the 400ms

following the detection of an SWR and peaking at 100ms after SWR detection (Figure 2f-g; Kruskal-Wallis ANOVA, post-hoc tests; gamma power > baseline; CA1: 0ms & 400ms, $p<0.05$; 100-300ms, peak, $p<10^{-5}$; CA3: 100-300ms, peak $p<0.001$).

The above results demonstrate that during SWRs there is a transient increase in gamma power and that the magnitude of this increase is correlated with the magnitude of the SWR. Next we asked whether the converse is true, that is, are increases in gamma power predictive of the presence of an SWR? Using a logistic regression generalized linear model (GLM), we found that gamma power in CA1 was significantly predictive of the presence of an SWR (CA1: 83% of sessions with significant GLM model, $p<0.05$). We illustrated this dependence by determining the probability that there was an ongoing SWR for different levels of gamma power. When CA1 gamma power exceeded 5 standard deviations above its mean, there was a 50% chance that there was a concurrent SWR and this probability increased with increasing gamma power (Figure 2h). Interestingly, there was no consistent relationship between CA3 gamma power and the probability of observing an awake SWR (Figure 2h). These results show that gamma oscillations are a consistent feature of SWRs and they suggest that SWRs occur when CA1 is entrained by ongoing gamma oscillations in CA3.

Does the transient increase in gamma power during SWRs reflect coupling between the CA3 and CA1 networks that could promote high fidelity replay of past experience? To address this question we asked whether the degree of gamma synchrony between CA3 and CA1 increases during SWRs. We examined synchrony using two related measures, phase locking and coherence. We first looked at gamma phase locking between CA3 and CA1. To compute gamma phase locking we measured the phase offsets over time between each pair of CA3 and CA1 tetrodes for each SWR. We then calculated the average phase offset across tetrode pairs for each SWR at each time. Phase locking describes the extent to which the phase offsets are consistent

across SWRs. Thus, a uniform distribution of phase offsets would have a phase locking value of 0 whereas the phase locking would be 1 if the phase offset between gamma oscillations recorded in CA3 and CA1 was the same value for each SWR.

As shown for an example run session, the distribution of phase offsets between gamma oscillations recorded in CA3 and CA1 sharpened at the time of SWR detections and peaked ~75ms after SWR detection, reflecting an increase in phase locking between regions (Figure 3a). Across sessions there was a significant increase in gamma phase locking between CA3 and CA1 for the 400ms following SWR detection (Figure 3b; Kruskal-Wallis ANOVA, post-hoc tests; gamma phase locking > baseline: 0-200ms, $p<10^{-5}$; 300-400ms, $p<0.001$). This increase in phase locking was also seen when analyses were restricted to CA3 and CA1 recording sites in different hemispheres, demonstrating that the transient synchrony we observe extends across hemispheres and was not simply due to volume conduction (Figure S3).

We next asked whether the magnitude of gamma coherence between CA3 and CA1 increased during SWRs. We found a transient increase of gamma coherence between CA3 and CA1 during SWRs (Figure 3c). Notably, as can be seen for this example run session, we observed no increase in the ripple band coherence during SWRs, replicating previous findings that ripple oscillations are not strongly coherent across CA3 and CA1 (Ylinen et al., 1995, Csicsvari et al., 1999) (Figure 3c). Gamma coherence between CA3 and CA1 was significantly greater than baseline values from 0 – 400 ms following SWR detection (Figure 3d; Kruskal-Wallis ANOVA, post-hoc tests; 0-400ms, peak $p<10^{-5}$; baseline CA3-CA1 coherence: 0.59). The increase in CA3-CA1 coherence was also present across hemispheres (Figure S3) and was accompanied by increases in cross-hemisphere CA3-CA3 and CA1-CA1 coherence (Figure S4). These findings indicate that during SWRs, gamma oscillations are transiently synchronized across the spatially distributed hippocampal network.

Could decreases in measurement error associated with the transient increase in gamma power during SWRs explain the transient increases in phase locking and coherence we observed? To control for this possibility we identified periods of CA1 gamma power associated with a 40-60% chance of SWRs (Figure 2h). When we compared the phase locking and the coherence magnitude of these gamma-power matched times for windows with (n = 2228) and without a SWR (n =16802), we found that phase locking and coherence were larger when an SWR was present than when it was not (gamma power matched coherence during SWRs, 0.73 ± 0.01 > no SWRs 0.69 ± 0.01; rank sum test, $p<10^{-5}$; gamma power matched phase locking during SWRs, 0.91 ± 0.03 > no SWR, 0.84 ± 0.03; rank sum test, $p<0.05$). Thus increases in gamma power alone cannot account for the greater gamma phase locking and coherence we observe during SWRs.

Gamma modulation of spiking during awake SWRs

If the increase in gamma coupling across regions during SWRs contributes to ordered replay of past experience, gamma phase would likely modulate SWR spiking. We examined spiking for CA3 (n = 8,351 spikes recorded from 123 neurons) and CA1 (n = 11,443 spikes recorded from 205 neurons) neurons separately as a function of the phase of the gamma oscillation recorded on a representative CA3 stratum pyramidale tetrode (see Methods). As individual neurons fired sparsely during, spikes were pooled across all putative excitatory neurons. We found that the spiking of putative excitatory neurons in both CA1 and CA3 was significantly phase locked to the phase of CA3 gamma oscillations during SWRs (Rayleigh tests: CA3 $p<0.01$, CA1 $p<10^{-5}$, Figure 4a). CA3 neurons fired preferentially near the peak of CA3 gamma (mean angle = 25 degrees) whereas CA1 neurons fired preferentially on the falling phase of CA3 gamma (mean angle = 114 degrees), a quarter of a cycle after CA3. CA3 firing occurred

significantly before the phase of CA1 firing (permutation test: $p<0.001$) at a timescale consistent with a monosynaptic delay between of ~8ms.

We then asked whether the transient increase in gamma coupling we observed earlier was associated with a transient increase in gamma modulation. We found that the depth of the gamma modulation of spiking in CA1 was twice as large during SWRs as compared to the 500ms preceding each SWR (Figure 4b; bootstrap re-sampling, depth of modulation during SWRs > depth of modulation preceding; $p < 0.001$). Interestingly, there was no change in the depth of modulation for CA3, indicating that CA3 neurons retain the same degree of gamma modulation before and during SWRs. The increase in modulation depth during SWRs for CA1 was also observed when we examined CA1 spiking relative to the gamma oscillation recorded on the local tetrode (depth of modulation preceding SWRs: 3%, depth of modulation during SWRs: 8%). These results indicate that during SWRs there is a transient increase in gamma coupling between CA3 and CA1 and this synchrony between regions entrain the spiking activity of the hippocampal output region CA1.

Replay events consist of the ordered spiking of CA3 and CA1 neurons during SWRs, and as CA3 drives downstream CA1 during these events, precise timing of CA3 spiking would be expected to be particularly important. During SWRs, neurons in CA3 and CA1 frequently fire in the context of multi-spike bursts (Buzsaki, 1986, Csicsvari et al., 2000), leading us to ask whether gamma modulated the onset of bursting. We found that gamma modulation was even more pronounced in CA3 when we included only the first spike each neuron fired during each SWR ($n = 3,287$ spikes from 123 neurons). Excluding all but the first spike each neuron fired during each SWR yielded a value for the depth of modulation of CA3 that was twice that seen when all spikes were included. Thus, the first spike from each CA3 neuron active during SWRs was strongly and significantly phase locked, with the proportion of spikes increasing during the rising

phase of gamma and the firing preferentially near the peak of gamma (preferred phase=-15 degrees, Rayleigh test, $p<0.01$; Figure 4c). The first spikes of CA1 neurons (n = 4,726 spikes from 205 neurons) were also significantly phase locked, with the spikes most likely to occur within a quarter cycle of gamma of the CA3 peak (preferred phase = 52 degrees, Rayleigh test, $p<0.01$). The depth of modulation for first CA1 spikes was similar to that seen for the inclusive CA1 spike analysis. Consistent with our results for all spikes, the first spike of CA3 neurons tended to occur before the first spike of CA1 neurons (permutation test: $p<0.05$). Taken together, these results suggest that gamma oscillations strongly modulate the onset of bursting in CA3 and couple CA1 to CA3 during SWRs.

Gamma modulation of awake replay during SWRs

During SWRs, previous experiences are replayed on a compressed timescale. Sequences of place cells that encode previously experienced paths through an environment are reactivated, replaying the sequences on a millisecond timescale during SWRs (Lee and Wilson, 2002, Foster and Wilson, 2006, Karlsson and Frank, 2009). As a result, pairs of cells with place fields close together in a previously experienced environment fire in close temporal proximity to one another during SWRs whereas pairs of cells with place fields far apart fire with longer inter-spike intervals(Karlsson and Frank, 2009) (Figure 5a; Spearman $\rho = 0.448$). If gamma provides a clock that synchronizes spiking in the CA3 and CA1 networks during SWRs, then relative gamma phase would provide the best measure of spike timing during SWRs.

Relative gamma phase and absolute time would be equivalent if gamma oscillations occurred at a constant frequency and were in perfect synchrony across the hippocampal network. However, while the correlation between relative spike timing and gamma phase is very high (Spearman $\rho = 0.98$), gamma frequency varies from cycle to

cycle (Atallah and Scanziani, 2009). Therefore, absolute time and gamma phase diverge when enough time has passed. This implies that any improvement in the description of spike timing using gamma as a clock will be most apparent at longer times / relative gamma phases. In contrast, if gamma oscillations do not act as a clock, then variations in gamma frequency across time would add noise to the reactivation of previous experience.

We therefore asked whether gamma phase better described pair-wise spiking structure during SWRs and how that related to the distance between place fields. We examined the structure of spiking consistent with remote replay of a previous run experience (Karlsson and Frank, 2009) and found that the relative gamma phase of spikes was significantly correlated with the distance between the place field peaks (Figure 5b, Spearman correlation: 0.46). This is slightly, but significantly, larger than the correlation between distance between place field peaks and spike timing (bootstrap test Spearman rho gamma > Spearman rho time; $p<0.05$). We then asked how the correlation between relative spike timing or change gamma phase with distance between field peaks varied as a function of distance between field peaks.

We divided place cell pairs into four equally sized groups and found that relative gamma phase and spike timing were both most correlated with distance for place fields with peaks far apart in space. Furthermore, for pairs of neurons with place fields farthest apart, the relative gamma phase was more correlated with distance than the relative time of spikes as measured in seconds (Figure 5c; bootstrap test, Spearman rho gamma > Spearman rho time; $p<10^{-5}$). These results suggest that gamma acts as a clock to synchronize the replay of stored memories across the hippocampal network.

Next we asked whether the strength of gamma synchrony was related to the presence of sequential replay of past experience. We reasoned that SWRs in which gamma synchronization of the CA3 and CA1 networks was greater should correspond to

SWRs in which sequential spiking activity could be most effectively maintained throughout the SWR. Bayesian population decoding yields a p-value describing the likelihood that the ordered firing seen during SWRs corresponded to a coherent trajectory through a previously experienced environment (Davidson et al., 2009, Karlsson and Frank, 2009). This p-value provides a measure of the quality of replay. Population decoding was restricted to candidate events defined as SWRs with at least 5 active cells that had place fields. Decoding was done with templates for both the animal's current W-track and where applicable, the previously experienced W-track environment, in order to minimize false negatives.

We found that phase locking of gamma oscillations between CA3 and CA1 varied as a function of replay p-value, with highly significant replay events displaying the strongest levels of gamma phase locking following SWR detection. The magnitude and the duration of gamma phase locking appeared to decrease as a function of the decoded significance of the replay event (Figure 6a). To quantify this observation we compared gamma phase locking between CA3 and CA1 for significant ($p<0.05$; n = 454 SWRs) and non-significant ($p>0.05$; n = 477 SWRs) candidate events and found significantly higher phase locking during significant events 50-250ms following SWR detection (Figure 6b; permutation test: significant phase locking > non-significant phase locking; $p<0.001$).

Similarly, the magnitude of the increase in gamma coherence between CA3 and CA1 strongly co-varied with the significance of memory replay. Highly significant replay events showed the biggest increase in coherence for the longest duration, less significant replay events showed a smaller increase in coherence for a shorter duration, and non-significant candidate events showed the smallest increase in coherence for the shortest duration (Figure 6c). As for gamma phase locking, the magnitude of gamma coherence between CA3 and CA1 was significantly different for significant ($p<0.05$) and

non-significant ($p>0.05$) candidate events for the 50-300ms after SWR detection (Figure 12d, permutation test: significant coherence > non-significant coherence; $p<0.001$). There were no consistent differences in either CA3 or CA1 gamma power based on with the presence of significant memory replay. Thus, while all candidate events involve activation of large populations of place cells during SWRs, stronger of gamma synchrony in the hippocampal network is predictive of the presence of coordinated memory reactivation during waking.

LFP Activity during quiescent SWRs

SWRs are prevalent during slow wave sleep and when animals are at rest. We have previously shown that reactivation occurring during quiescent SWRs occurring in rest periods tend to be a less faithful recapitulation of patterns from previous awake experience than activity during awake SWRs (Karlsson and Frank, 2009). We therefore asked whether gamma synchronization during quiescent SWRs, defined as SWRs that occurred in the rest box when animals had been still for more than 60 seconds, differed from gamma synchronization seen during awake SWRs. As observed for awake SWRs, quiescent SWRs were accompanied by transient increases in gamma power in CA1 and CA3 (Figure 7a-b; Kruskal-Wallis ANOVA, post-hoc tests; gamma power > baseline power; CA1 -100ms - 400ms, peak $p<10^{-5}$; CA3 0-400ms, peak, $p<10^{-5}$). There was also a small but non-significant increase in gamma phase locking between CA3 and CA1 during quiescent SWRs accompanied by a small but significant increase in gamma coherence (Figure 7c-d; Kruskal-Wallis ANOVA, post-hoc tests; phase locking > baseline, NS; gamma coherence > baseline, 0ms, 200-400ms $p<0.05$, 100ms, $p<10^{-5}$).

Interestingly, the smaller magnitude of the increase in gamma synchrony during quiescent SWRs as compared to awake SWRs could be explained in large part by an increased baseline gamma synchrony during quiescence. The average gamma phase

locking and coherence preceding SWRs was higher during quiescent SWRs (Figure 7e-f; phase locking baseline quiescent SWRs > awake SWRs; rank sum test; $p<10^{-5}$, coherence baseline quiescent SWRs > awake SWRs; $p<10^{-5}$). Furthermore, while gamma synchrony reached a slightly higher level during quiescent SWRs as compared to awake SWRs (Figure 7e-f; phase locking 100ms following SWR detection quiescent > awake; rank sum test, $p<10^{-5}$; coherence 100ms following SWR detection; quiescent > awake; rank sum test, $p<10^{-5}$), the higher baseline synchrony means that SWR associated increases reflected a smaller change than seen during awake periods. The higher baseline suggests the possibility that gamma synchrony across the hippocampal network acts as a gate for the occurrence of SWRs, with more synchronous network states (e.g. quiescence) resulting in a lower threshold for the occurrence of SWRs and less synchronous network states (e.g. awake) requiring more synchronous drive from CA3 in order to initiate an SWR.

Gamma modulation of spiking and replay during quiescent SWRs

Do gamma oscillations clock the replay of previous experiences when animals are at rest? As observed during awake SWRs, the spiking of putative excitatory neurons in both CA1 (n = 10,952 spikes recorded from 270 neurons) and CA3 (n = 6,848 spikes recorded from 226 neurons) was significantly phase locked to the phase of gamma during quiescent SWRs (Figure 7g; Rayleigh test, CA3 $p<0.05$; CA1 $p<0.05$). However, there was no significant difference in the modulation of either CA3 or CA1 spiking during SWRs as compared to the 500ms preceding SWR detection, suggesting that the high baseline values of gamma synchrony maintain gamma phase locking throughout periods of quiescence.

We then asked how gamma phase was related to the reactivation of representations of past experience during quiescent SWRs. As for awake SWRs, we

computed the correlation between the distance between field peaks recorded during the preceding behavioral sessions and the relative spike timing or gamma phase during quiescent SWRs. As previously reported (Karlsson and Frank, 2009, Dupret et al., 2010a), the correlations during quiescent SWRs were lower than those in the awake state (Figure 7g; permutation test, awake > quiescent Spearman ρ; distance between place field peaks vs. relative spike timing and distance between place field peaks vs. gamma phase $p<0.001$). Nonetheless, relative gamma phase was more correlated with distance between place field peaks than the relative spike timing (Figure 7h; bootstrap test, Spearman ρ gamma > Spearman ρ time; $p<0.05$). Thus, as we observed for awake SWRs, gamma oscillations during quiescent SWRs coherently modulates the hippocampal circuit and could act as a clock to synchronize the replay of stored memories. Finally we asked whether the strength of gamma synchrony during quiescent SWRs in the rest session was correlated with the presence of replay. In contrast to our results for awake SWRs, we found no consistent relationship between the increase in gamma synchrony during quiescent SWRs and the presence of significant replay. This may be a result of the smaller increases in gamma phase locking and coherence during quiescent SWRs and the overall lower fidelity of quiescent replay.

Discussion

Previous studies have examined the structure of local field potential and spiking activity within SWRs, but the patterns of activity that synchronize large populations of CA1 and CA3 neurons across hemispheres have remained unclear. We examined the structure of LFP activity associated with SWRs occurring during both awake and quiescent states and found a prominent and consistent increase in power in the 20-50 Hz gamma band during SWRs. During this transient increase in power, gamma

oscillations in CA3 and CA1 became more coherent both within and across hemispheres, indicating a transient synchronization of the entire dorsal hippocampal network. Spikes from neurons in both CA3 and CA1 were phase locked to the common gamma rhythm during SWRs and relative gamma phase, rather than absolute time, better described the structure of pair-wise spiking during SWRs. Further, during awake SWRs, higher levels of gamma phase locking and coherence across CA3 and CA1 were associated with higher fidelity replay of past experience. These results suggest that gamma modulation of spiking is important for maintaining the temporal organization of spiking during the reactivation of stored memories in the hippocampal network.

Our results also revealed interesting differences between awake and quiescent SWRs that may be related to the lower fidelity of replay seen during quiescence as compared to awake states (Karlsson and Frank, 2009, Dupret et al., 2010b). We have also shown that there are overall levels of network activation during quiescent, as compared to awake SWRs (Karlsson and Frank, 2009), but the reason for these differences has not been clear. Here we found that during awake SWRs there were larger increases in gamma synchrony during SWRs than seen during quiescence, a difference that could be largely attributed to the higher baseline levels of synchrony during quiescence. Transient increases in gamma synchrony during awake SWRs were associated with strong phase modulation of the initial spikes from CA3 neurons and a substantial increase in the modulation of all spikes from CA1 neurons. Thus during awake SWRs, CA3 neurons tended to begin spiking near the peak of the CA3 gamma and CA1 neurons became strongly phase locked to the same gamma oscillation, firing approximately a quarter cycle later. Further, higher fidelity awake replay was associated with stronger gamma phase locking and coherence across the CA3 and CA1 networks. In contrast, CA1 and CA3 neurons were phase locked to gamma to the same degree before and during quiescent SWRs. There was also no evidence for a clear relationship

between phase locking or coherence and the fidelity of quiescent replay. These findings demonstrate that there are differences in the baseline state of the network in the awake and quiescent states. We suggest that the higher baseline levels of gamma phase locking and coherence during quiescence contribute to the broader network activation and lower fidelity replay seen in the quiescent state.

Our results suggest that current models describing the generation of ripples (Traub and Bibbig, 2000, Memmesheimer, 2010, Taxidis et al., 2011) need to be modified to account for the prominent gamma oscillations during SWRs. These models have proposed various mechanisms to account for the prominent high frequency ripple modulation in CA1, but none have posited a lower frequency gamma rhythm that transiently binds the CA3 and CA1 networks during SWRs. At the same time, our findings are entirely consistent with previous studies of gamma. Models have shown that gamma rhythms are well suited to synchronize networks with relatively low conduction delays (Kopell et al., 2000) as in the densely connected CA3-CA1 network. Gamma has also been shown to improve information transmission in cortical networks (Sohal et al., 2009), consistent with our observation of stronger gamma synchrony for significant awake replay events.

Previous studies of gamma in the hippocampus have largely focused on gamma in the context of the theta rhythm which modulates activity during awake exploration (Bragin et al., 1995, Jensen and Lisman, 1996, Chrobak and Buzsaki, 1998, Lisman and Otmakhova, 2001, Csicsvari et al., 2003, Montgomery and Buzsaki, 2007, Montgomery et al., 2008, Colgin et al., 2009). Our result demonstrates that 20-50 Hz slow gamma is present not only during theta, but is also prominent during SWRs, which occur most often when animals are still and theta is low amplitude or absent (Buzsaki et al., 1983). Thus, slow gamma may be a signature of a specific type of hippocampal information processing.

What functions could gamma support? We and others have suggested that replay during awake SWRs could support awake memory retrieval (Karlsson and Frank, 2009, O'Neill et al., 2010, Carr et al., 2011). The strong gamma synchrony we found during awake memory replay provides a new connection between replay and previous studies linking gamma oscillations to memory encoding (Fell et al., 2003, Osipova et al., 2006, Jutras et al., 2009, Tort et al., 2009, Fell and Axmacher, 2011) and retrieval (Lisman and Otmakhova, 2001, Montgomery and Buzsaki, 2007). In particular, one model proposed that gamma rhythms seen during awake exploration and theta are well suited to clock the retrieval of sequential memories in the hippocampus (Lisman and Otmakhova, 2001). Consistent with that idea, more recent work demonstrated that CA3 – CA1 gamma coherence was enhanced during movement through a part of a maze where animals had to make memory-guided decisions (Montgomery and Buzsaki, 2007). Similarly, CA3 gamma is prevalent at times associated with vicarious trial and error activity (Johnson and Redish, 2007) that are strikingly similar to awake replay events. Further, the lower frequency gamma enhanced during SWRs has been shown to couple the CA3 and CA1 networks (Colgin et al., 2009). When viewed in the context of these previous findings, our results strongly suggest that there is a specific pattern of enhanced CA3-CA1 gamma power, phase locking, and coherence that is a consistent signature of awake memory retrieval in the hippocampal network, both when animals are still and when they are exploring. These gamma oscillations are well suited to promote accurate retrieval of sequential memories and may also contribute to the entrainment of neurons downstream regions such as entorhinal or prefrontal cortex.

Our findings also suggest a prominent role for fast-spiking interneurons that express the calcium-binding protein parvalbumin in memory reactivation. Parvalbumin positive interneurons play an important role in the generation of cortical and hippocampal gamma oscillations (Bartos et al., 2007, Tukker et al., 2007, Cardin et al.,

2009, Sohal et al., 2009) and have also been shown to be active during SWRs in vivo (Klausberger et al., 2003). Thus, similar mechanisms may support gamma oscillations that occur during both in the context of theta and SWRs. Intriguingly, selective suppression of PV+ interneurons in the mouse hippocampus results in a working memory deficit (Murray et al., 2011). We would predict that the synchronization of the CA3 and CA1 networks was impaired in these animals, leading to a selective deficit in their ability to generate sequential memory replay.

The link between gamma and memory replay in the hippocampus complements a broad array of studies linking enhanced gamma synchrony in information processing, object recognition, sensory processing, top-down control, and attention (Womelsdorf et al., 2007, Cardin et al., 2009, Jutras et al., 2009, Sohal et al., 2009, Fell and Axmacher, 2011). These studies showed that increases in gamma power and synchrony are associated with better sensory processing for external stimuli. Our results link gamma to internally generated patterns of activity that can be independent of sensory input, and suggests that gamma synchrony across the hippocampus plays a central role in the coherent reactivation of memories.

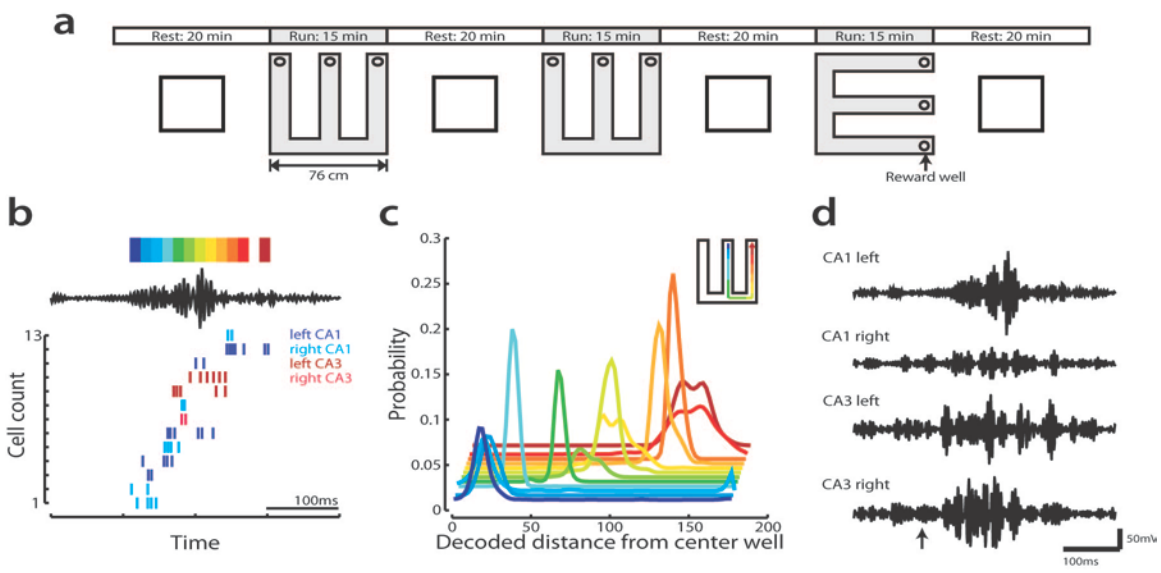

Figure 1 | Memory reactivation can reflect spatially distributed neural populations. **(a)** Schematic of recording paradigm. SWRs were recorded while animals were performing a spatial alternation task in one of two initially novel W-tracks (76cm along each dimension) and during interleaving sessions in a rest box (25cm x 34cm). **(b)** Sequential spiking of neurons during awake, remote replay of the first W-track. This SWR occurred when the animal was located in the second W-track. Top, filtered (150-250Hz) local field potential signal from one CA1 tetrode. The color bar shows the colors associated with each of the 15ms decoding bins. Bottom, spike rasters of all neurons with place fields in the first W-track that were active during the SWR. Colors indicate the region and hemisphere of each active neuron. **(c)** Decoded locations for each 15ms bin. Each colored line represents the probability distribution in space resulting from decoding. Inset, a cartoon of the replayed trajectory. **(d)** Increases in ripple amplitude can occur concurrently across CA1 and CA3 and across hemispheres but have different structure at each recording site. Shown is the example SWR shown in b-c. Arrow indicates time of SWR detection.

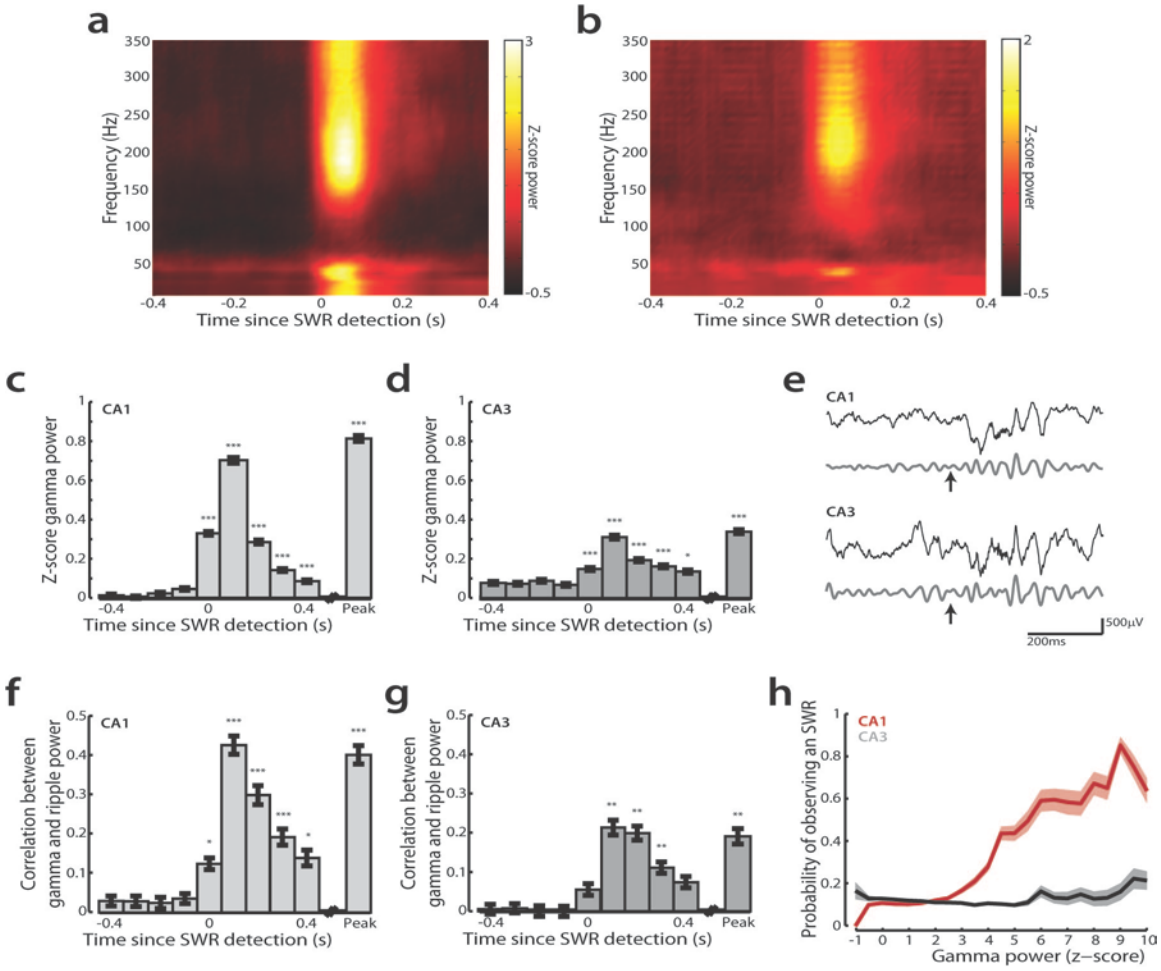

Figure 2 | Transient increases in gamma power are concurrent with SWRs. **(a-b)** Average **(a)** CA1 and **(b)** CA3 SWR triggered spectrograms from one example behavioral epoch from animal 3. Spectrograms have been averaged across SWRs and stratum pyramidale tetrodes. Gamma power is shown as a z-score computed for each frequency band across the entire behavioral session. **(c-d)** Quantification of gamma power for the 400ms before and after SWR detection and at the peak ripple power for **(c)** CA1 and **(d)** CA3. All error bars are s.e.m. unless otherwise noted. **(e)** Broadband LFP (1-400Hz) and gamma filtered LFP (20-50Hz) for a representative SWR (same as in **Fig. 3b-d**). Arrow indicates time of SWR detection. **(f-g)** Quantification of the correlation between gamma power and CA1 ripple power on an SWR-by-SWR basis in 100 ms bins before and after SWR detection and at the peak ripple power for gamma recorded in **(f)** CA1 and **(g)** CA3. **(h)** Probability of observing an SWR as a function of CA1 (red) or CA3 (black) gamma power. Solid lines show means, filled lines show standard error of the mean across sessions. * $p < 0.05$; ** $p < 0.001$; *** $p < 10^{-5}$.

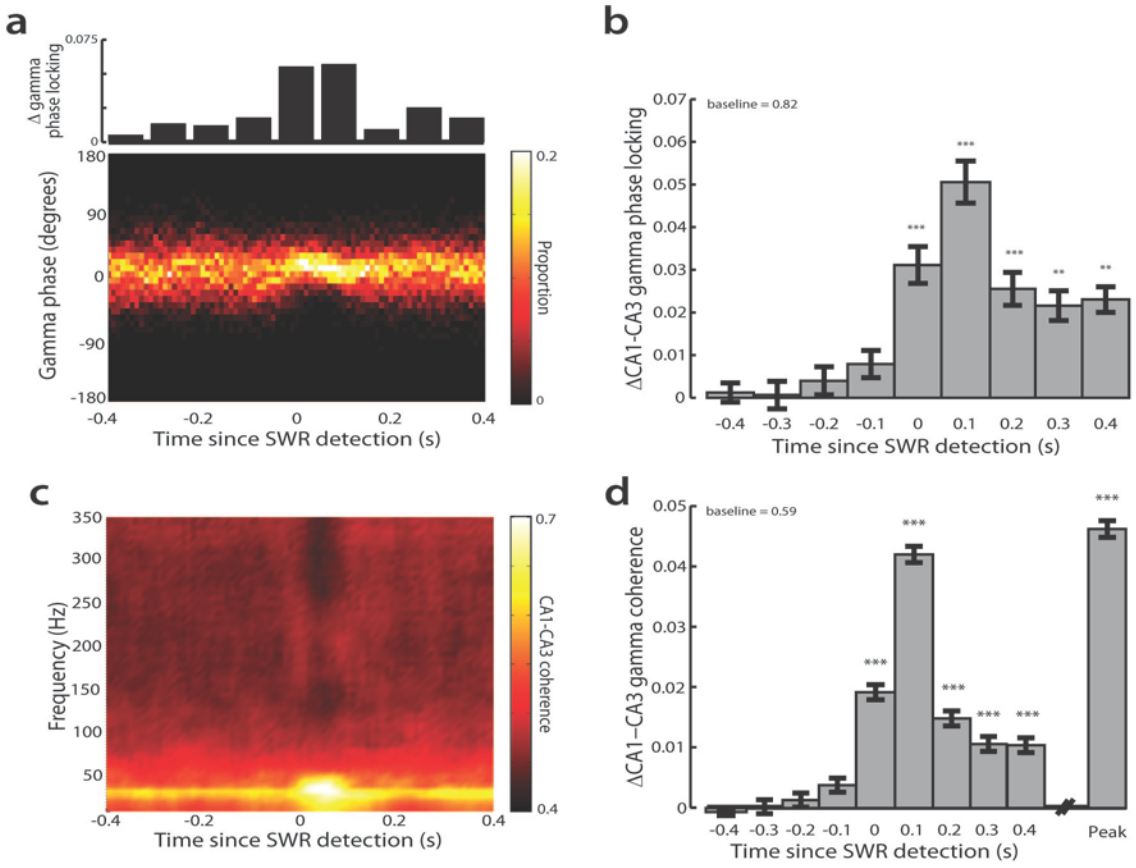

Figure 3 | During SWRs, gamma oscillations between CA3 and CA1 become transiently synchronized. **(a)** Bottom, distribution of phase offsets between gamma oscillations recorded in CA3 and CA1 for times around SWR detection for a representative run session (same behavioral session as **Fig. 4a-b**). Top, change in gamma phase-locking from baseline (450-400ms before SWR detection) for this example session. **(b)** Average gamma phase locking between CA3 and CA1 across all sessions. Average value for gamma phase-locking baseline is given at top. **(c)** Average magnitude of coherence between CA3 and CA1 (same behavioral session as in a). Note the increase in gamma coherence for the 150ms following SWR detection. **(d)** Quantification of change in gamma coherence between CA3 and CA1 across time and at the peak ripple power. Average value for gamma coherence baseline is given at top. ** $p<0.001$; *** $p<10^{-5}$.

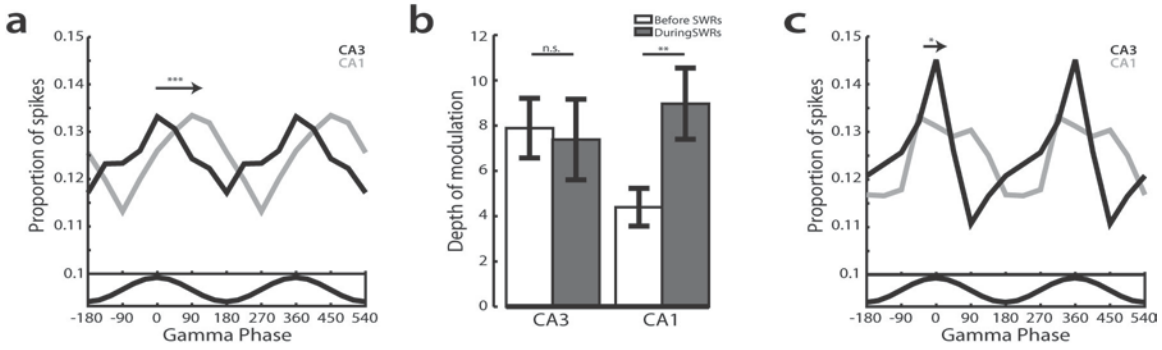

Figure 4 | Gamma oscillations during SWRs entrain spiking in CA3 and CA1. **(a)** Spiking in CA3 (black) and CA1 (grey) is modulated by ongoing gamma oscillations. Arrow denotes difference between CA3 and CA1 mean phase. Bottom, average gamma trace across phases. **(b)** Quantification of modulation depth for the 500ms before SWRs (white) and during SWRs (grey). **(c)** Gamma phase modulations for the first spike fired during each SWR for both CA3 (black) and CA1 (grey). Arrow denotes difference between CA3 and CA1 mean phase. * $p<0.05$; ** $p<0.001$; *** $p<10^{-5}$.

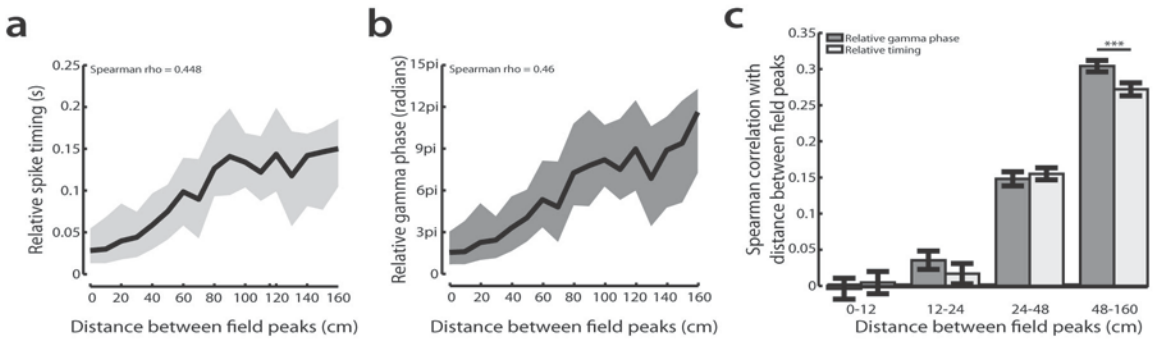

Figure 5 | Gamma oscillations can provide a clock for memory reactivation. **(a)** Pair-wise reactivation of neurons with place fields on a previously experienced W-track are reactivated during awake SWRs. Neurons with place fields close together fire in close temporal proximity whereas neurons with place fields further apart fire at longer intervals. **(b)** Pair-wise reactivation can also be observed when using relative gamma phase of spikes instead of absolute time. **(c)** The correlation between place field distance and relative gamma phase or spike timing varies as a function of distance between place field peaks. Gamma phase is a better descriptor of pair-wise reactivation than absolute time for place fields located far apart on the track. *** $p<10^{-5}$.

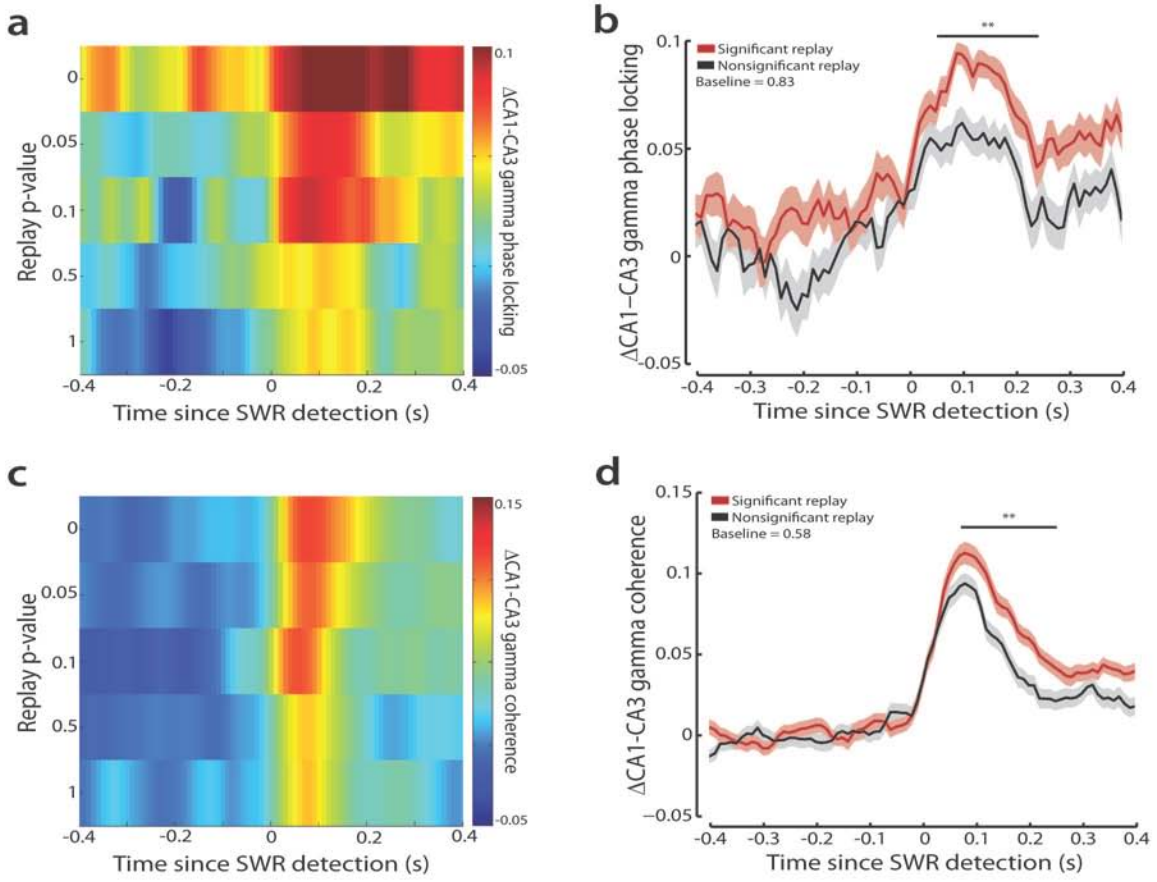

Figure 6 | Significant replay is associated with stronger gamma synchrony between CA3 and CA1 during SWRs. **(a)** Gamma phase locking between CA3 and CA1 varies as a function of replay p-value. **(b)** There is a larger increase in gamma phase locking for significant as compared to non-significant candidate events. Solid lines show means, filled lines show standard error of the mean across candidate events. **(c)** Gamma coherence between CA3 and CA1 varies as a function of replay p-value. **(d)** There is a larger increase in gamma coherence for significant as compared to non-significant candidate events. Solid lines show means, filled lines show standard error of the mean across candidate events. ** $p<0.001$.

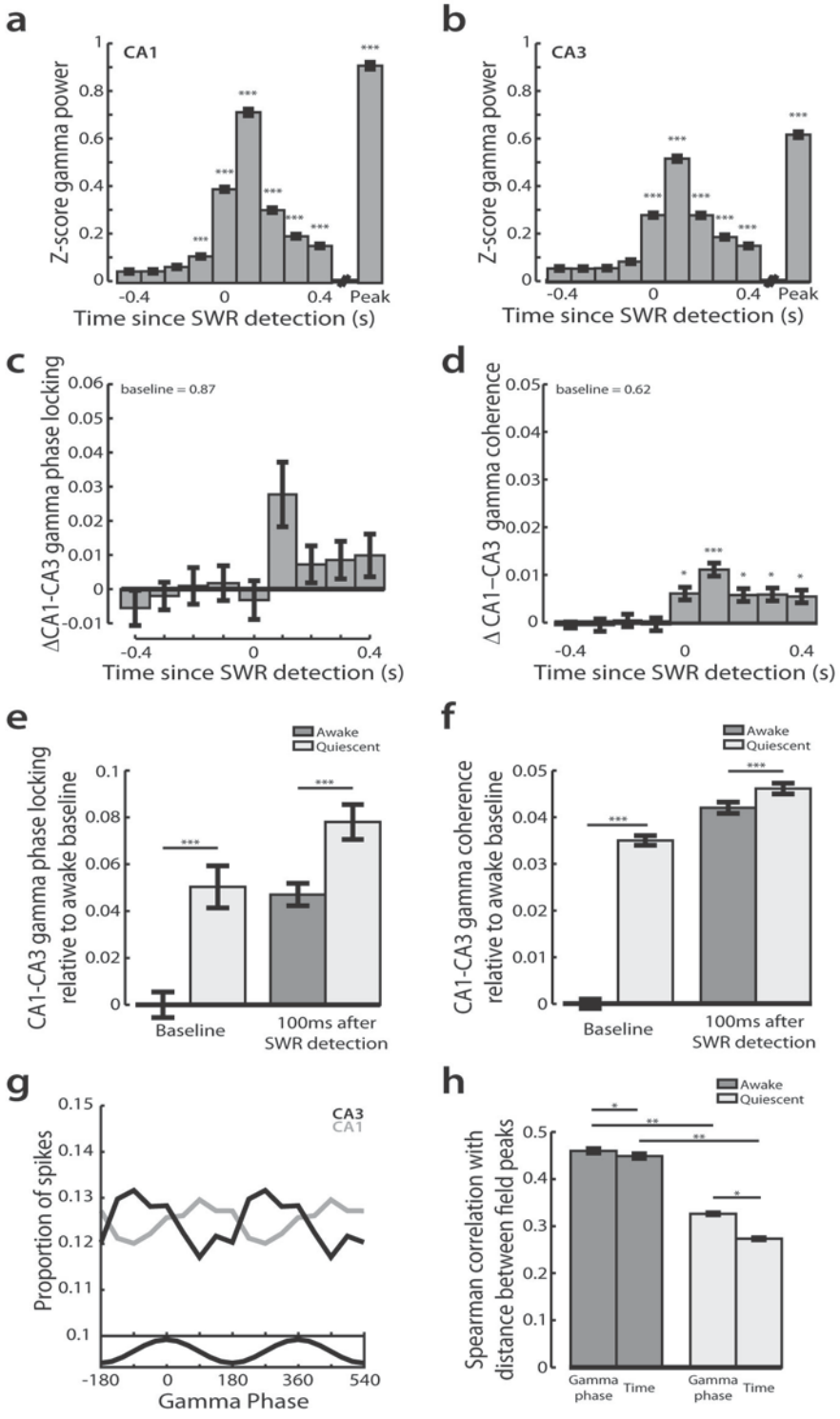
a
CA1
Z-score gamma power
Time since SWR detection (s)
Peak
b
CA3
Z-score gamma power
Time since SWR detection (s)
Peak
c
baseline = 0.87
ΔCA1-CA3 gamma phase locking
Time since SWR detection (s)
d
baseline = 0.62
Δ CA1–CA3 gamma coherence
Time since SWR detection (s)
e
Awake
Quiescent
CA1-CA3 gamma phase locking relative to awake baseline
Baseline
100ms after SWR detection
f
Awake
Quiescent
CA1-CA3 gamma coherence relative to awake baseline
Baseline
100ms after SWR detection
g
CA3
CA1
Proportion of spikes
Gamma Phase
h
Awake
Quiescent
Spearman correlation with distance between field peaks
Gamma phase
Time
Gamma phase
Time

Figure 7 | Transient increases in gamma oscillations during quiescent SWRs. **(a—b)** Gamma power for the 400ms before and after quiescent SWR detection and at the peak ripple power for **(a)** CA1 and **(b)** CA3. **(c)** Change in gamma phase locking between CA3 and CA1 for the times around quiescent SWR detection. Average value for gamma phase-locking baseline is given at top. **(d)** Change in gamma coherence between CA3 and CA1 for the 400ms before and after quiescent SWR detection. Average value for gamma coherence baseline is shown at top. **(e-f)** Comparison between awake (dark grey) and quiescent (light grey) states for baseline **(e)** gamma phase locking and **(f)** gamma coherence as well as **(e)** gamma phase locking and **(f)** gamma coherence observed 100ms following SWR detection. Values are plotted relative to mean awake baseline levels. **(g)** Spiking in CA3 (black) and CA1 (grey) is modulated by ongoing gamma oscillations. **(h)** Correlation between place field distance and relative gamma phase or spike timing is stronger during awake SWRs (dark grey) as compared to quiescent SWRs (light grey). For both awake and quiescent SWRs, gamma phase is a better descriptor of pair-wise reactivation than absolute time. * $p<0.05$; ** $p< 0.001$; *** $p<10^{-5}$.

Supplemental Figures

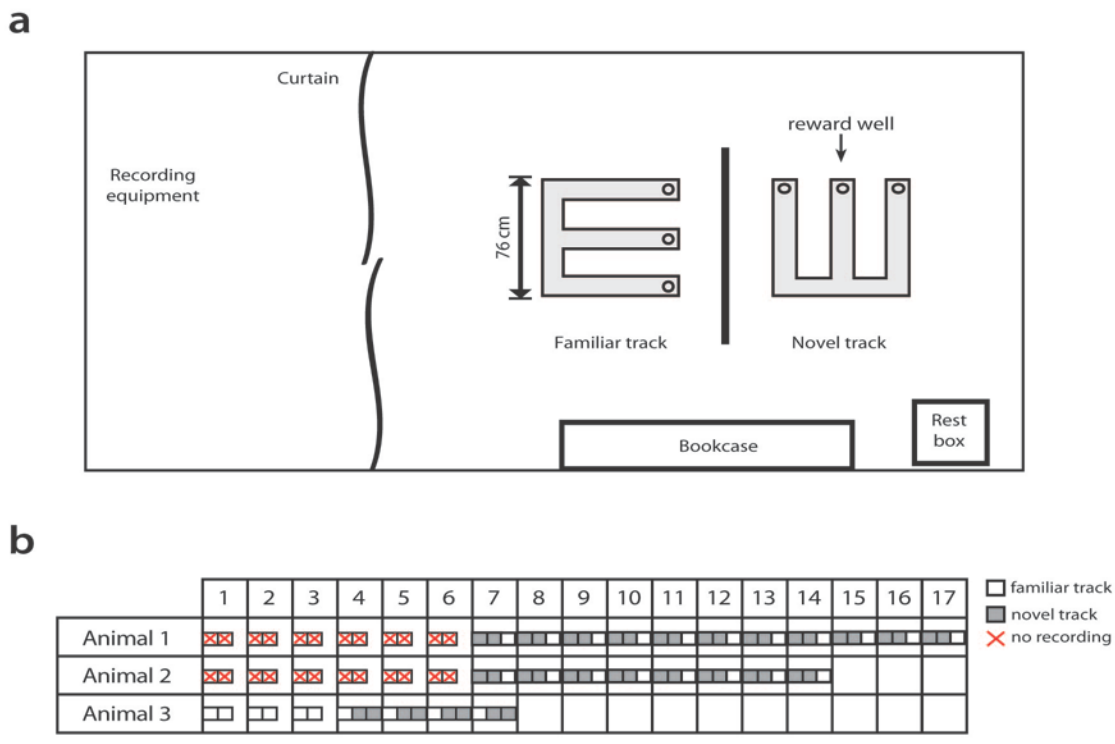

Figure S1 | Experimental setup. **(a)** Layout of W-tracks and rest box in the recording room. A high barrier separated the two W-tracks so that one was not visible from the other. The two tracks were in visually distinct contexts as there were prominent visual cues including the rest box, a curtain, and a bookcase. **(b)** Behavioral and recoding schedule for each animal across days. White squares indicate a 15 minute run on the more familiar W-track, grey squares indicate a run on the more novel W-track, and red marks indicate behavior only days. Twenty minute sessions in the rest box preceded and followed each run sessio

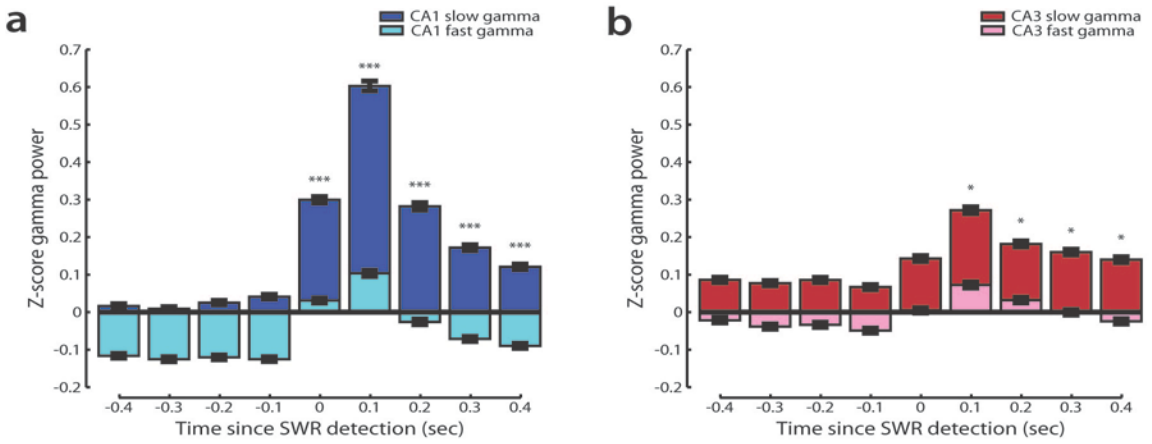

Figure S2 | Transient increases in slow gamma power (20-50Hz) are significantly larger than increases in fast gamma power (60-100Hz). **(a-b)** Slow and fast gamma power is shown as a z-score computed for each frequency band across the entire behavioral session. Quantification of gamma power for the 400ms before and after SWR detection for **(a)** CA1 and **(b)** CA3. Slow gamma power is greater than fast gamma power for all times and there was a significant increase in the difference between slow and fast gamma power during SWRs as compared to baseline (Kruskal-Wallis ANOVA, post-hoc tests; slow gamma power – fast gamma power > slow gamma power- fast gamma power at baseline). *$p<0.05$; *** $p<10^{-5}$.

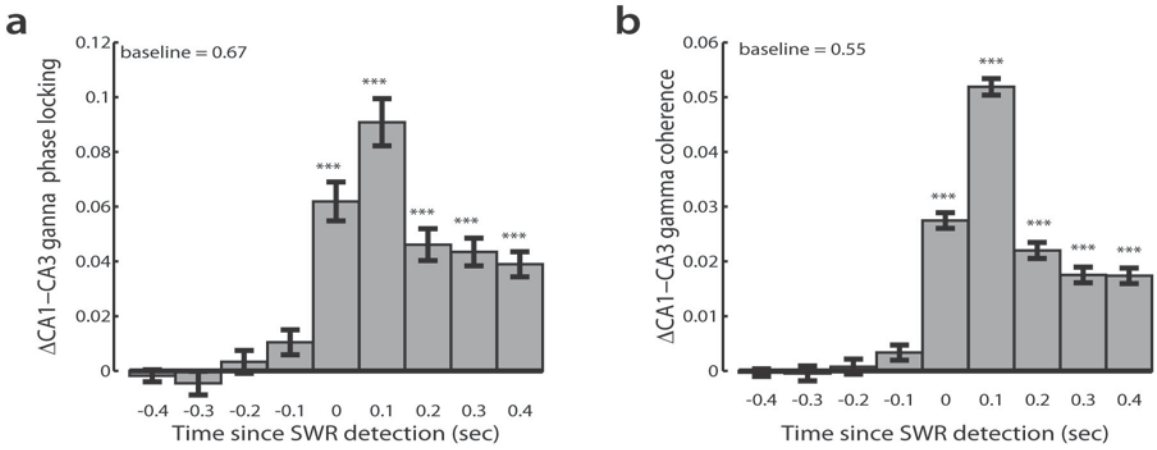

Figure S3 | During SWRs, gamma oscillations between CA3 and CA1 become transiently synchronized across hemispheres. **(a)** Quantification of change in gamma phase locking between CA3 and CA1 recorded in opposite hemispheres for the 400ms before and after SWR detection. Average value for gamma phase-locking baseline is shown at top. **(b)** Quantification of change in gamma coherence between CA3 and CA1 recorded in opposite hemispheres for the 400ms before and after SWR detection and at the peak ripple power. Average value for gamma coherence baseline is shown at top. *** $p<10^{-5}$.

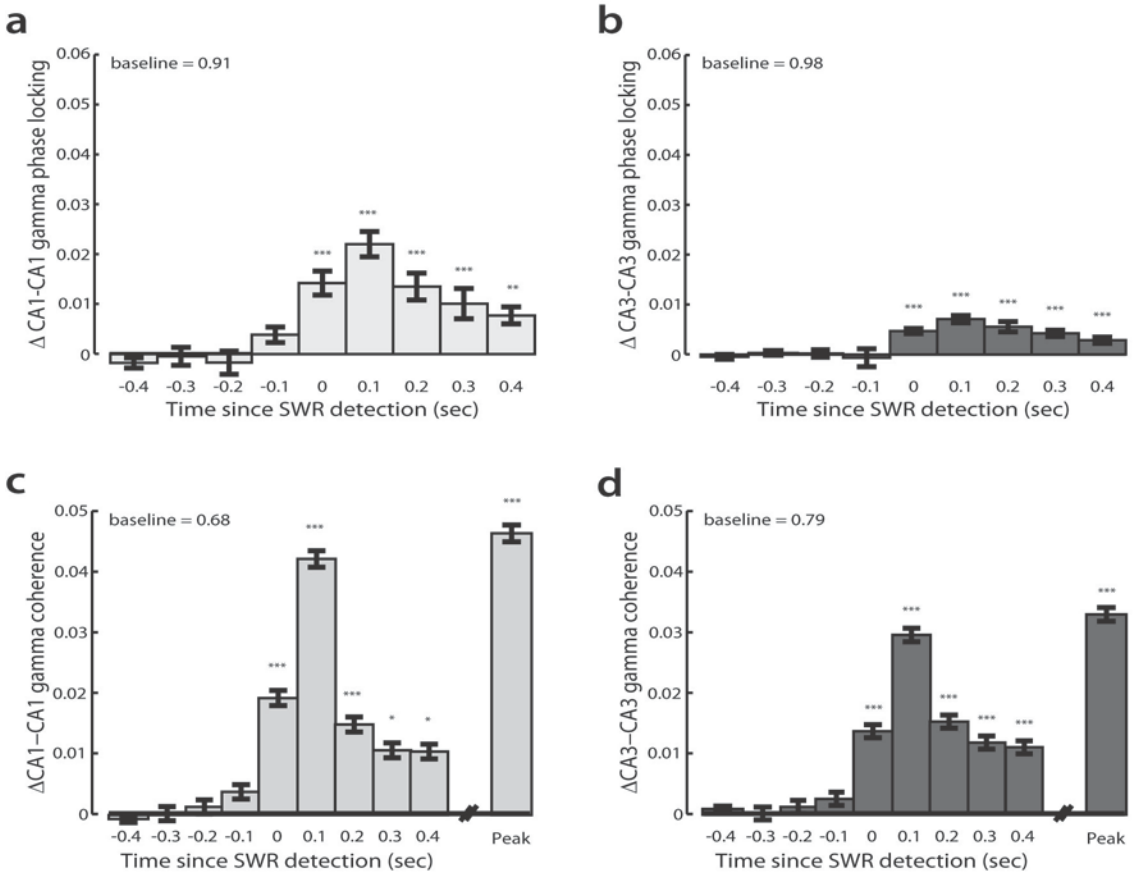

Figure S4 | During SWRs, gamma oscillations within hippocampal subregions become transiently synchronized. **(a-b)** Quantification of change in gamma phase locking between **(a)** CA1 recorded in opposite hemispheres and **(b)** CA3 recorded in opposite hemispheres for the 400ms before and after SWR detection. Average value for gamma phase-locking baseline is shown at top. Note gamma oscillations within hippocampal subregions are very synchronous at baseline. **(c-d)** Quantification of change in gamma coherence between **(c)** CA1 recorded in opposite hemispheres and **(d)** CA3 recorded in opposite hemispheres for the 400ms before and after SWR detection and at the peak ripple power. Average value for gamma coherence baseline is shown at top. * $p<0.05$; ** $p<0.001$; *** $p<10^{-5}$.

Methods

Unique sets of analyses of the data used in this study and the associated methods have been presented previously (Karlsson and Frank, 2008, 2009).

Data collection

Three male Long-Evans rats (500-600g) were pre-trained to run back and forth on a linear track for liquid reward (sweetened condensed milk) and food deprived to no less than 85% of their baseline weight during behavioral training. Animals were implanted with a microdrive containing 30 independently movable tetrodes targeting anatomically connected regions of CA3 and CA1 bilaterally (Karlsson and Frank, 2008, 2009) following University of California San Francisco Institutional Animal Care and Use Committee and US National Institutes of Health guidelines. At the end of data collection electrolytic lesions were made and electrode locations were identified histologically (Karlsson and Frank, 2008).

On each recording day, animals performed two or three 15 minute run sessions in W-track environments (76cm x 76cm with 7cm wide track sections) with 20 minute rest sessions in a high walled box (floor 25cm x 34cm; walls 50cm tall) before and after each run. The first W-track environment was introduced either 6 (n = 2) or 3 (n = 1) days before animals were introduced to the second W-track (Figure 4). Rats were rewarded for performing a continuous alternation task (Frank et al., 2000, Karlsson and Frank, 2008, 2009). Rapid learning in this task requires an intact hippocampus(Kim and Frank, 2009).

Data were collected using the NSpike data acquisition system (L.M.F. and J. MacArthur, Harvard Instrumentation Design Laboratory). An infrared diode was attached to the preamps during recording. Following recording, the rat's position on the track was

reconstructed using a semi-automated analysis of digital video of the experiment. Spike data were recorded relative to a reference tetrode located in the corpus callosum, sampled at 30KHz, digitally filtered between 600Hz and 6KHz (2 pole Bessel for high and low pass), and threshold crossing events were saved to disk. Local field potentials were recorded relative to a ground screw located above the cerebellum, sampled at 1.5KHz, and digitally filtered between 0.5Hz and 400Hz. Individual units (putative single neurons) were identified by clustering spikes using peak amplitude and spike width as variables (MatClust, M.P.K.). Only well-isolated neurons with stable spike wave forms were included.

Analysis

Analyses were carried out using custom software written in Matlab (Mathworks) and the Chronux toolbox (http://www.cronux.org). SWRs were identified on the basis of peaks in the LFP recorded from tetrodes in the CA1 stratum pyramidale. For all analyses, tetrodes were defined as being in stratum pyramidale using post-mortem histology and the presence of at least 2 putative excitatory neurons. The raw LFP data was band pass filtered between 150-250Hz and the SWR envelope was determined using a Hilbert transform. The envelope was smoothed with a Gaussian (4ms standard deviation). SWR events were identified as times when the smoothed envelope was above 3 standard deviations from mean for at least 15ms on at least one CA1 tetrode. The entire SWR event was defined as including times immediately before and after that prolonged threshold crossing event during which the envelope exceeded the mean (Cheng and Frank, 2008). We restricted our analyses of awake SWRs to times when the animal was moving less than 4cm s^{-1} in either W-track and our analyses of quiescent SWRs to times when the animal as in the rest box and had been immobile for at least one minute. We excluded any SWR that occurred in a one second following detection of another SWR so

that no SWRs occurred during the baseline period. Behavioral or rest sessions with fewer than five SWRs were excluded from analyses. All analyses used non-parametric comparisons because the distributions were non-normal.

Gamma power

SWR triggered spectrograms were computed using the multi-taper method from the Chronux toolbox. Multi-taper estimates of the power spectrum were computed using 100ms windows and a z-score was computed for each frequency band using the mean and standard deviation of the power calculated across the entire behavioral session for each tetrode. Thus for each 100ms bin, we obtained a normalized measure of power for each frequency band in units of standard deviations from the mean for each tetrode. For illustration in figures, power was computed using 10ms sliding windows. To quantify the increase in gamma power during SWRs, the z-scored power in the gamma band (20-50Hz) was averaged across all CA1 or CA3 tetrodes. Baseline was defined as values between 450 and 400ms before SWR detection. As 100ms temporal bins were used to compute all spectral analyses, to determine the significance of gamma increases we asked how gamma power levels at 100 ms intervals compared to baseline values. To compute the correlation between gamma and ripple power, power in the ripple band (150-250Hz) was averaged across all CA1 tetrodes. The Spearman correlation between ripple power and CA1 or CA3 gamma power was taken for each behavioral session and the correlation coefficient was compared in 100ms intervals to baseline values.

Generalized Linear Model

We used a generalized linear model with a logistic link function (also known as logistic regression) to determine whether gamma power was predictive of the presence of an SWR. The average gamma power across CA1 or CA3 tetrodes was computed across

the entire behavioral session using 200ms temporal bins. For each 200ms bin we also determined whether or not an SWR was observed. Gamma power was said to predict the occurrence of an SWR for behavioral sessions with significant coefficients. To illustrate the relationship between gamma power and the occurrence of an SWR, we binned gamma power and then computed the proportion of 200ms bins that had an SWR.

Gamma synchrony

SWR triggered coherence was computed for all CA3-CA1 tetrode pairs using the multi-taper method from the Chronux toolbox using 100ms windows. Briefly, coherence provides an estimate for the extent to which one signal can be predicted by another and is a ratio of the cross spectrum divided by the product of the individual spectra. For illustration in figures, coherence was computed using a 10ms sliding windows.

To quantify gamma phase locking during SWRs, the phase of coherence for the gamma band (20-50Hz) was averaged across all CA3-CA1 tetrode pairs for each SWR. Thus for 100ms temporal bin relative to SWR detection there was a single value per SWR. We combined values across SWRs to obtain a distribution of gamma phase offsets in each bin. Phase locking for each bin is a measure of the concentration of distribution of phases, calculated by creating a unit vector pointing in the direction of each member of the distribution, summing the unit vectors and normalizing the result. This measure of phase locking will be one if the phase offset is equal for every SWR and zero if the phase offsets are uniformly distributed. Phase locking was computed for all behavioral sessions with at least five SWRs. To determine the significance of gamma phase locking increases we asked how phase locking at 100ms intervals compared to baseline. To quantify the magnitude of gamma coherence during SWRs, we computed the absolute

value of the average coherence in the gamma band (20-50Hz) across all CA3-CA1 tetrode pairs. To determine the significance of increases in gamma coherence compared the magnitude of coherence at 100ms intervals to baseline values.

Spiking modulation by gamma oscillations

Gamma phase was measured on the CA3 tetrode with the largest number of isolated cells by band pass filtering (20-50Hz) the local field potential, performing the Hilbert transform on the filtered signal, and extracting the phase component. Spikes that occurred during an SWR were identified and the gamma phase at the time of the spike was assigned. As the firing during SWRs is very sparse, spikes were pooled across neurons recorded in either CA3 or CA1. The depth of modulation was defined as the difference between the peak and the trough of the spiking distribution divided by the sum of the peak and the trough of the spiking distribution. The depth of modulation for spikes that occurred in the 500ms before SWR detection was computed in order to determine the baseline gamma modulation of spiking in area CA3 and CA1. We used bootstrap re-sampling to compute error bars on the depth of modulation.

Pair-wise reactivation

As in our previous work (Karlsson and Frank, 2009), for every pair of place fields we measured the linear distance between the place field peaks as the shortest path between the peak firing rate locations. We also measured the absolute value of both the time and gamma phase from each reference spike for one cell to all spikes from the other cell. For this analysis, relative gamma phase was determined by determining how many cycles of gamma had elapsed between spikes on the CA3 tetrode with the most cells. Only spikes occurring during SWRs and only times up to 500ms were included. We then computed the Spearman's correlation between linear distance and either

relative spike timing or gamma phase to determine how strongly these measures co-varied. Each pair of cells was included only once. To determine the relationship between place field distance and correlation with gamma phase and spike timing, we divided the data into roughly four equally sized groups based on the distance between place field peaks. We then computed the spearman's correlation between linear distance and either relative spike timing or gamma phase for each group. We used bootstrap resampling to compute error bars on the correlations.

Decoding

To measure place field locations, we calculated an occupancy-normalized linearized place field for each cell, calculated in 2-cm bins and smoothed with a 4-cm standard deviation Gaussian curve. Only times outside of SWRs were included. The place field peak rate was defined as the maximum rate across all spatial bins. A peak rate of 3Hz or greater was required for a cell to be considered a place cell. Putative interneurons were identified on the basis of spike width and average firing rate (Ranck, 1973, Fox and Ranck, 1981, Frank et al., 2000) and were excluded from all analyses.

Candidate replay events were defined as SWRs during which at least five place cells from the replayed environment fired at least one spike each. We determined the sequential representation of position seed during a candidate replay event using a simple Bayesian decode that has been described in detail before (Karlsson and Frank, 2009). Briefly, each event was divided into 15ms bins and for each bin with at least one spike in it, we calculated the spatial probability distribution using an uninformative prior.

To determine whether the temporal sequence of decoded spatial probability distributions was a significant memory replay we compared the regression of spatial locations with temporal bin to 10,000 regressions in which the order of the bins was shuffled. The P

value for each candidate event was defined as the proportion of the shuffled R^2 values that was greater than the R^2 value of the actual event, and an event with $p<0.05$ was considered to be significant.

To ask how gamma phase locking and coherence varied as a function of replay significance, we separated candidate events by the replay p-value. We computed the phase locking and average coherence across significant and non-significant events. We used a permutation test to determine when the difference between significant and non-significant candidate events was significant. We compared the measured difference to the difference computed on 1,000 permutations on the p-value associated with each candidate event.

Chapter 2

Continuous network states in the hippocampus

Abstract

Hippocampal information processing is often described as two-state, with a place cell state during movement and a reactivation state during stillness. Here we show that hippocampal processing is better described as a continuum. We measured the relationship between moment-by-moment changes in behavior and information flow through hippocampal output area CA1 in rats. We examined local field potential (LFP) patterns, ensemble spiking, and evoked potentials associated with internal drive from CA3 to CA1. We found that there was a smooth transition from strong to weak CA3 drive of CA1 as animals moved progressively more quickly. LFP patterns associated with external entorhinal cortical drive of CA1 showed the opposite pattern, increasing in strength with increasing speed. Behavioral modulation of both CA3- and entorhinal-driven patterns of activity was most pronounced in novel environments. Our results suggest that CA1 output represents a continuously changing balance between CA3-driven learned associations and independent sensory representations.

Introduction

Hippocampal activity is required for both laying down the memories of ongoing experience and converting these initial, labile traces into long lasting distributed representations (Squire, 1992, Cohen and Eichenbaum, 1993). Standard models of hippocampal function have posited two distinct network states associated with these processes (Buzsaki, 1989). The creation of new memory traces is thought to occur

during active exploration when the ~8 Hz theta rhythm is prominent and hippocampal place cells are active in specific regions of the animal's environment. During this state, highly processed sensory information from the entorhinal cortex (EC) drives activity throughout the hippocampal circuit (Bragin et al., 1995, Brun et al., 2008).

In contrast, the consolidation process that leads to the formation of stable long term memories is thought to occur during periods of awake stillness or slow-wave sleep. At these times, sharp-wave ripple (SWR) events are prominent in hippocampal output area CA1 (Buzsaki, 1986). These events generally occur when bursts of activity generated in upstream hippocampal area CA3 propagate out through CA1 (Buzsaki et al., 1983, Csicsvari et al., 2000, Sullivan et al., 2011). In the absence of sensory input, the highly plastic and recurrent CA3 is thought to act as an auto-associative pattern completion network (Marr, 1971, McNaughton and Morris, 1987, Amaral et al., 1990) that can reinstate learned patterns. Neural activity during SWRs frequently involves replay of stored sequences associated with past experience (Lee and Wilson, 2002, Foster and Wilson, 2006, Diba and Buzsaki, 2007, Karlsson and Frank, 2009), and interrupting SWRs following learning is sufficient to impair subsequent performance (Girardeau et al., 2009, Ego-Stengel and Wilson, 2010), indicating that SWRs contribute to memory consolidation.

These two network states are thought to reflect at least in part the strength of the Schafer Collateral (SC) pathway from CA3 to CA1. Measures of field EPSP slope indicate that the effective strength of CA3 input to CA1 is substantially reduced when animals are running as compared to periods of immobility (Segal, 1978, Winson and Abzug, 1978, Leung, 1980). Thus, strong CA3 input to CA1 is associated with the still/consolidation state while weak CA3 input to CA1 is associated with the moving/encoding state.

While this framework dominates current thinking about hippocampal activity, a number of findings do not fit well within the two state model. In addition to its role in memory consolidation, CA3 input to CA1 is important for one-trial learning in a novel context (Nakashiba et al., 2008) which need not occur during periods of stillness. Furthermore, recent work has identified slow (~20-50 Hz) and fast (~50–100 Hz) frequency ranges of the gamma rhythm in CA1 that correspond respectively to CA3 or EC coherence with CA1 (Colgin et al., 2009). Both ranges of gamma were seen during exploration, suggesting that CA3 influence can be strong during movement. Finally, during new experiences when the hippocampus is critical for forming memories, rats exhibit complex, exploratory behaviors (O'Keefe and Nadel, 1978, Lever et al., 2006) that are not well understood as either “moving” or “still”. These new experiences lead to stronger reactivation, and that reactivation can be seen both when animals are moving and when they are still (O'Neill et al., 2006, Cheng and Frank, 2008).

These results suggest the possibility of more nuanced relationship between behavior and information processing in the hippocampus. This led us to investigate the dynamics of the CA3-CA1 network as a function of behavior during learning. We found that movement speed continuously modulates the influence of CA3 on activity in CA1. As animals move faster, the influence of CA3 on CA1 decreases as measured by the amplitude of SWRs, the power of slow gamma oscillations, and the synaptic strength of the CA3-CA1 pathway. The level of coordinated spiking activity in CA1 reflects the influence of CA3: cell assemblies are highly correlated at low speeds and become progressively less correlated with increasing movement speed. In contrast, the power of the fast gamma oscillations that link EC and CA1 increased with speed. These results are not compatible with a two state model but instead suggest that movement speed

drives a dynamic balance between learned associations and more independent sensory representations in the hippocampus.

Results

Continuous changes in hippocampal LFP during exploration

We investigated the influence of CA3 on CA1 while rats learned a hippocampally-dependent spatial alternation task in an initially novel W-shaped maze (Figure 1a; Figure S1) (Frank et al., 2000, Karlsson and Frank, 2008, Kim and Frank, 2009). Both the maze and the available distal cues were entirely novel when animals were first exposed to the environment. We used head-mounted light-emitting diodes to track head movement in the plane of the maze and estimated two-dimensional movement speed by smoothing the temporal derivative of position with a Gaussian with a standard deviation of 0.5 seconds (see Methods). As expected, animals initially spent more time exploring the environment. A signature of this exploration was an increase in periods when the rats moved at intermediate two-dimensional speeds (Figure 1b). Intermediate speeds were only weakly correlated with speed along the axis of the track (Figure 1c; no significant changes in correlations with experience). This indicates that the rats did not simply move towards goal locations more slowly in novel environments; rather, movement at intermediate speeds reflects exploratory behavior, as opposed to linear, goal directed motion. As the environment became more familiar, the distribution of movement speed shifted rightwards as animals spent more of their time running quickly between goal locations (Figure 1b).

The two state model predicts a sharp transition in hippocampal network function as animals start moving, corresponding to the transition from SWR to theta dominated local field potential (LFP) activity. We tested that prediction by examining the LFP

recorded in CA1 during the first exposure to the novel W task. We observed striking and continuous changes in the power spectrum of the LFP recorded in CA1 *stratum pyramidale* as a function of movement speed (Figure S2). We found that movement speed was correlated with the power in three physiologically relevant frequency ranges (Figure 2), two associated with CA3 drive: slow gamma (~20-55Hz) and ripple (150-250 Hz) oscillations, and one associated with EC drive: fast gamma oscillations (~65-140 Hz). As seen in this example, with increasing speed in the novel environment there was an apparent decrease in the power of rhythms associated with CA3 input and a concurrent increase in the power of EC associated fast gamma. The tradeoff between CA3 and EC associated patterns occurred smoothly as a function of speed, in contrast to the predictions of the two state model. To quantify these observations, we investigated the modulation of each frequency band separately.

Smooth modulation of gamma power during learning

We began with an examination of slow and fast gamma oscillations (Colgin et al., 2009) during the first exposure to a novel environment. We replicated previous observations that CA3 and CA1 are most coherent at slow gamma frequencies (~20-55Hz) while EC and CA1 are most coherent at fast gamma frequencies (~65-140Hz; Figure S3) (Colgin et al., 2009). These findings have been interpreted to indicate that periods of increased slow gamma power in CA1 are indicative of greater CA3 drive, while increases in fast gamma power are indicative of greater EC drive (Bragin et al., 1995, Colgin et al., 2009). We found that the power of slow gamma was largest when the animal was still and decreased smoothly with the log of speed (Figure 3a; bootstrap linear regression, normalized slow gamma power vs. log(speed); $p < 10^{-5}$). Further, when we binned speed logarithmically, speeds of 1, 4, and 16 cm/sec were all associated with significantly different levels of slow gamma power (Kruskal-Wallis ANOVA, post-hoc

tests, $p < 0.01$). In sharp contrast, the power of fast gamma oscillations continuously increased with increasing speed (Figure 3b; bootstrap linear regression, normalized fast gamma power vs. log(speed); $p < 10^{-5}$). Fast gamma power was significantly different between all non-adjacent speed bins (Kruskal-Wallis ANOVA, post-hoc tests, $p < 10^{-5}$). This finding is consistent with previous reports of positive correlation between high gamma power and speed (Chen et al., 2011) and slightly higher average speeds associated with fast as compared to slow gamma (Colgin et al., 2009).

Does the modulation of slow and fast gamma power by speed reflect moment-by-moment changes in behavior? If so, then the timescale of changes in gamma power should match the timescale of changes in movement speed. We first calculated the autocorrelations of movement speed and found that speed changes rapidly from second to second (Figure 3c). We then computed the cross-correlation between gamma power and speed. If gamma power reflected extended timescale changes in behavior (i.e., "moving" and "still"), then the cross correlation would fall off gradually. In contrast, we find that the correlation between speed and gamma power is largest when the speed and gamma power are measured at the same time (lag = 0), and decreases rapidly with increasing lags (Figure 3c; correlation decreases below 95% bootstrap confidence interval for offsets > 0.5 s). The similarity between the timescales of change in behavior and in cross correlation between gamma and speed suggests that there is a strong coupling between moment-by-moment movement and the power of gamma oscillations in CA1 on the timescale of a second.

We found the same pattern of rapid change in gamma power when we examined periods of acceleration or deceleration. We isolated two second segments of behavior in which the rat was rapidly changing speed, either increasing from less than 2 cm/s to more than 10 cm/s or decreasing from more than 10 cm/s to less than 2 cm/s. We then

examined the power of fast and slow gamma during these events. When rats accelerated slow gamma power decreased and fast gamma power increased (Figure 3d, 87 events in 6 rats, ANOVA, interaction term and post-hoc tests of initial vs. final power, $p < 10^{-5}$). Conversely, as rats decelerated, slow gamma power increased and fast gamma power decreased (Figure 3e; 152 events in 6 rats, all comparisons again $p < 10^{-5}$). These observations were robust to the duration and speed criteria used to identify acceleration and deceleration events. Thus, rapid changes in speed correspond to rapid alterations in the relative balance between slow and fast gamma. These findings suggest that the coupling of CA1 with both CA3 and EC changes with moment-by-moment alterations in behavior.

Our results indicate that the speed that a rat moves is a parsimonious and temporally precise predictor of the relative intensity of fast and slow gamma oscillations in CA1. As speed is a behavioral measure, we also considered the possibility that a commonly used physiological measure, the power of the theta rhythm, could provide a more accurate prediction than speed. The theta (7-9 Hz) rhythm is prominent in rodent hippocampus and the power of theta increases with movement speed (Whishaw and Vanderwolf, 1973, Rivas et al., 1996, Buzsaki, 2002, Montgomery et al., 2009). The correlation between theta power and speed (Figure S4; $R^2 = 0.17$) suggests that theta power could be a better predictor of moment-by-moment variations in gamma power than movement speed. However, during the first novel exposure we found that correlation between speed and slow and fast gamma power is nearly twice that of the correlation between theta and gamma power (Figure 3f, pooled data: $\rho_{speed} > \rho_{theta}$, bootstrap p's < 0.01 for both slow and fast gamma; $p < 0.05$ for 5 of 6 animals individually). Thus during novel exploration, speed is a better predictor of gamma power than theta power.

As an environment becomes more familiar, animals begin to move faster, engaging in more goal directed movement. Activity patterns in CA1 change over this same time period, reflecting the development of stable representations (Wilson and McNaughton, 1993, Frank et al., 2004, Karlsson and Frank, 2008). These changes in behavior and CA1 output as well as the particular importance of area CA3 for rapid learning lead us to ask whether the influence of speed on the slow and fast gamma bands associated with CA3 and EC input to CA1 changed with experience. We found that the speed modulation of slow and fast gamma power was strongest during exploration of a novel environment and decreased with increasing familiarity. There was a two-fold change in the correlation between speed and gamma power between the first and tenth exposure to an initially novel environment for both slow and fast gamma (Figure 3g; permutation test, exposure vs. slope; slow gamma, $p < 10^{-5}$; fast gamma, $p < 10^{-5}$). This was observed for both the group data and for each individual animal (permutation test, exposure vs. slope; p's < 0.01). The introduction of a second novel environment led to greater modulation of both slow and fast gamma as a function of speed and was associated with an overall increase in both slow and fast gamma power as compared to that seen on the more familiar track (see Methods; Figure S5). The weakening relationship between gamma power and speed as the environment became more familiar may explain why a recent study found a positive relationship between slow gamma and speed in mice (Chen et al., 2011).

Thus, there is a smooth shift from slow to fast gamma as animals move more quickly, which is most pronounced in novel environments but remains when the environment is familiar. In conjunction with the evidence that slow gamma reflects CA3 – CA1 coupling while fast gamma reflects EC – CA1 coupling (Colgin et al., 2009) our results suggests that in contexts in which the hippocampus is strongly engaged, the

balance of CA1 inputs from CA3 to EC changes continuously as a function of movement speed. These results are not compatible with a simple two-state model but instead indicate that there is a smooth continuum related to the relative influence of internal CA3 versus external EC drive of CA1.

Smooth modulation of CA1 ripple oscillations

We then asked whether ripple oscillations in CA1 also showed a smooth modulation as a function of movement speed. Ripple oscillations generally reflect synchronized CA3 input (Csicsvari et al., 2000) and are associated with the replay of previously stored memories (Wilson and McNaughton, 1993, Lee and Wilson, 2002, Foster and Wilson, 2006, Diba and Buzsaki, 2007, Karlsson and Frank, 2009). Just as for the CA3-related slow gamma oscillation, we found that during the first exposure to a novel environment, the power of ripple oscillations was largest when the animal was still and decreased smoothly with speed (Figure 4a; bootstrap linear regression, normalized ripple power vs. log(speed); $p < 10^{-5}$). We also found that the power of ripple oscillations was most strongly modulated as a function of speed in a novel environment and decreased as the environment became more familiar. There was a three-fold change in slope between the first and tenth exposure to an initially novel environment (Figure 4b; permutation test, exposure vs. slope; $p < 10^{-5}$). The enhancement of speed modulation in a novel environment was present in both the group data, for each individual animal and for within day comparisons (permutation test, exposure vs. slope, p's $< 10^{-5}$; Figure S6). Furthermore, as expected (Cheng and Frank, 2008), novelty was associated with an overall increase in ripple power (Figure S6).

During ripple oscillations, sets of place cells reflecting previous experiences are frequently reactivated. This reactivation supports memory storage (Girardeau et al., 2009) and may additionally support memory retrieval (Karlsson and Frank, 2009, O'Neill

et al., 2010, Carr et al., 2011). We asked how speed affected neural activation during ripple oscillations. We found that CA1 neurons were most likely to fire during ripples that occurred at slow speeds and became progressively less likely to fire during ripples that occurred at faster speeds (Figure 4c; bootstrap linear regression, activation probability vs. log(speed), $p < 10^{-5}$). In contrast, while neurons in CA3 were active during ripples detected in CA1, we found no significant correlation between movement speed and activation probability for CA3 (Figure 4c; bootstrap linear regression, activation probability vs. log(speed); $p > 0.1$). Finally, we found that specifically in CA1, activation probability during ripples was largest during novel experiences and decreased as the environment became more familiar. In contrast the activation probability in CA3 remained stable across time (Figure 4d; permutation set, exposure vs. slope; CA1 $p<10^{-5}$; CA3 $p > 0.1$).

Thus, in a novel environment, rhythms in CA1 associated with CA3 input, both ripple and slow gamma power, are strongly modulated as a function of speed. These results indicate that CA3 input to CA1 is modulated by movement speed and novelty across the full dynamic range of behavior. Furthermore, these results suggest that modulation of CA3 input could explain previous observations of greater memory reactivation during and after new experiences (Cheng and Frank, 2008, O'Neill et al., 2008). Interestingly, the activity of neurons *within* CA3 during ripple oscillations showed no modulation by either speed or novelty. This is particularly surprising given that this population activity in CA3 is thought to initiate ripple oscillations (Buzsaki et al., 1983, Csicsvari et al., 2000, Nakashiba et al., 2009) and suggests that CA3 activity is relatively independent of speed but that the impact of CA3 output on CA1 changes smoothly with movement speed.

Smooth modulation of SC pathway strength

Does the smooth modulation of ripples and slow gamma reflect smooth modulation of the strength of the Schafer Collateral (SC) pathway from CA3 to CA1? The SC pathway is weaker in moving as compared to still rats (Segal, 1978, Leung, 1980). However, it is unknown how the strength of the SC pathway varies on a moment-by-moment basis during behavior. To determine whether speed-related changes in the strength of the SC pathway were sufficient to produce the physiological effects we observe, we measured evoked field responses to electrical stimulation of the SC pathway. We chronically implanted biphasic stimulating electrodes in either contralateral CA3 or in the commissural CA3 fibers (see Methods). Stimulation yielded similar patterns of activation, so we combined data across stimulation sites.

We found that the slope of the field excitatory post-synaptic potential (fEPSP), showed a remarkable level of variation, by as much as 200%, which was very strongly correlated with the animals' instantaneous movement speed. The evoked fEPSPs in area CA1 decreased smoothly with increasing movement speed, with intermediate speeds corresponding to an intermediate synaptic strength (Figure 5a; linear regression, fEPSP slope vs. log(speed); $F(328)=305$, $p < 10^{-5}$, $R^2 = 0.48$). This was true both for individual epochs and when normalized responses were pooled across behavioral epochs and animals (Figure 5b; Figure S7; 31 epochs from 4 animals, linear regression, normalized fEPSP slope vs. log(speed); $F(2770)=616$, $p < 10^{-5}$, $R^2 = 0.18$). We found that fEPSP slopes were significantly different across all non-adjacent speed bins (Kruskal-Wallis one way ANOVA, post-hoc tests, p's < 0.05), such that speeds of 0.25, 1, 4 and 16 cm/sec were all associated with progressively and significantly weaker SC input to CA1. These results demonstrate that hippocampal information processing cannot be meaningfully divided into two distinct states on the basis of behavior.

The slope of the fEPSP is frequently used as a measure of synaptic strength (Bliss and Lomo, 1973, Winson and Abzug, 1978, Whitlock et al., 2006), but multiple factors can influence fEPSP slope in-vivo, and so we considered how changes in factors other than synaptic strength would affect the interpretation of our results. For example, increased fEPSP amplitude in the dentate gyrus region can result from increases in temperature associated with exploration (Moser et al., 1993). Temperature is not a viable explanation for our results, however, as we found that CA1 fEPSP slope was largest when animals were still, when brain temperature would be expected to be lowest. We also considered the possibility that post-synaptic membranes were progressively more depolarized at higher speeds, leading to a decrease in the driving force and thus a decrease in fEPSP strength. While depolarization of neurons could lead to small changes in driving force, the magnitude of depolarization observed *in vivo* (Epsztein et al., 2011) is too small to account for the large changes we observed as a function of speed. We also reasoned that modulation of the SC pathway was unlikely to be due primarily to SC input onto interneurons based on interneuron morphology and the numbers (Freund and Buzsaki, 1996). Thus, the measured change in fEPSP slope is best understood as a change in the strength of the SC pathway.

On what timescale do changes in movement speed correlate with changes in the strength in the SC pathway? We computed the correlation between speed and SC pathway strength as a function of the temporal offset between the speed and fEPSP measurements (Figure 5c). As for gamma power, speed was most predictive of SC strength at short timescales and the correlation decreased significantly for offsets of more than ±0.75 sec (bootstrapped 95% confidence interval; Figure S7). We next asked whether theta power could better explain the smooth modulation of synaptic strength than speed. We measured the R^2 of the linear relationship between the fEPSP slope and

theta power. Again, speed was a consistently better predictor of the strength of the SC pathway than theta (Figure 5d; pooled data, bootstrap $p < 0.001$, rank sum test across epochs, $p < 0.001$, $p < 0.05$ for 29 of 31 epochs individually). These results demonstrate that the strength of the SC pathway is modulated continuously as a function of moment-by-moment alterations in speed. These rapid alterations in the strength of the SC pathway are ideally suited to contribute to the rapid modulation of ripple and slow gamma power we observed in CA1.

Smooth modulation of correlated neural activity in CA1

Increasing speed is associated with a decrease in the strength of the CA3 inputs to CA1. Furthermore, as the CA3 input decreases in strength, there is a transition from CA3-associated slow gamma to EC-associated fast gamma and a decrease in the amplitude of CA3-driven ripple oscillations in CA1. How does this decrease in CA3 drive with increasing speed impact place cell activity in CA1?

CA3 is necessary for forming new representations and generating reactivation of previous experiences, suggesting that spiking in CA3 reflects learned associations (Nakashiba et al., 2008, Nakashiba et al., 2009). The role of CA3 in memory-related activity is most apparent in the reactivated sequences observed during CA3 driven ripple oscillations (Diba and Buzsaki, 2007, Girardeau et al., 2009, Karlsson and Frank, 2009, Nakashiba et al., 2009), but the effect of changes in the strength of the CA3 input to CA1 in the context of place cell activity has not been examined. We hypothesized that CA3 input drives the expression of correlated activity in CA1 place cells, reflecting learned associations, and that this correlated activity would reflect the strength of the CA3 input to CA1. To investigate correlated population activity, we excluded ripple events and examined the structure of CA1 place cell activity. We asked how the correlation of residuals (Singer et al., 2010) between pairs of cells with overlapping place fields varied

with speed and novelty. The residual correlation (or “noise correlation”) is a measure of how moment-by-moment variability in firing rate co-varies between cell pairs. Cell pairs with strong residual correlations are likely to be part of functional cell assemblies (Harris et al., 2003), whereas cell pairs with small residual correlations fire more independently and this de-correlated activity may be more informative to downstream targets.

We found that the distributions of residual correlations during the first two days of experience differed markedly across speeds (Figure 6a; KS test all pairs: $p<10^{-5}$). To quantify these differences, which consisted of both larger positive and larger negative correlations at low speeds as compared to high speeds, we asked how the absolute value of the residual correlation coefficients, the coordination index, varied across speed. We found that the coordination index was largest at slow speeds and decreased smoothly as animals moved faster (Figure 6b). There was an approximately three-fold decrease in coordinated activity from the slowest to the fastest speed bin, and comparisons across all speed bins were highly significant (Kruskal-Wallis ANOVA, post-hoc tests, $p < 10^{-5}$). Thus, pairs of co-active neurons had higher residual correlations at slow speeds and became progressively de-correlated as animals moved faster. These results could not be explained by a correlation between the animal’s movement speed and the residuals themselves (Figure S8). Furthermore, the speed modulation of residual correlations was apparent when using shorter timescales (125 ms), when we restricted measurements to within the place fields (minimum spatial firing rate of 1Hz), and for cell pairs with every combination of peak firing rates (Figure S8).

We next asked how novelty modulated the correlation of residuals. We found that in a familiar environment, there was an overall increase in the residual correlation, consistent with previous results showing that residual correlations increase with learning (Singer et al., 2010) (rank sum test, novel vs. familiar residual correlations for all speeds,

$p < 10^{-5}$). However, this overall increase was due to increases specifically at higher speeds (Figure 6c; rank sum test; 4 cm/second novel vs. familiar; $p < 0.05$; 16cm/second novel vs. familiar, $p < 10^{-5}$). Thus while over time, correlations of cell pairs increased, the relationship between speed and correlated firing was strongest when animals were exploring a novel environment. This suggests that during exploration of a novel environment, correlated firing in CA1 reflects the rapid associations formed in the CA3 recurrent network when the SC pathway to CA1 is strong at slower speeds. As the environment becomes more familiar, the correlated activity in CA1 may reflect both correlated input from CA3 and associations which have been learned by the network over time. Interestingly, the analysis by speed revealed a much larger dynamic range of coordination levels than the same analysis applied to periods with increased slow or fast gamma power (Figure 6c), demonstrating that speed is a better predictor of the structure of CA1 output than gamma frequency. Taken together, these findings indicate that the structure of CA1 spiking changes markedly as a function of movement speed, with the strongly correlated activity seen at low speeds when the influence of the highly recurrent CA3 network is greatest giving way to more independent activity as speed increases.

Discussion

Our results indicate that as animals behave in a novel environment, the speed of their head movement is a simple and parsimonious indicator of the influence of the recurrent CA3 network on CA1. We found that changes in CA3-associated patterns – slow gamma and ripple power – occur on the same timescale as changes in the underlying strength of the SC pathway, directly measured via the slope of evoked fEPSPs. This suggests that speed-dependent modulation of the SC is partially responsible for the changes we observe in CA1 activity. While CA1 activity related to

CA3 decreases with increasing speed, we found a concomitant increase in the power of EC-associated fast gamma oscillations (Bragin et al., 1995, Colgin et al., 2009). Increasing fast gamma power could simply reflect decreased CA3 input or potentially an additional modulatory influence of speed on the strength of the direct input from EC layer III or indirect cortical input from EC layer III through hippocampal area CA2 (Chevaleyre and Siegelbaum, 2010). The output spiking activity of CA1 reflected the smooth speed-dependent dynamics seen in gamma and ripple oscillations. At low speeds where CA3 input dominates, CA1 neurons were much more likely to be activated during ripple events and residual correlations of pairs of CA1 neurons were high. At higher speeds CA1 neurons tended to fire more independently, consistent with a decreasing influence of correlated activity from CA3. In a novel environment, animals spend less time moving quickly and more time at intermediate speeds, effectively increasing the influence of the recurrent CA3 network on CA1. In addition to this behavioral bias, novelty itself increases the influence of CA3 to CA1, particularly at low speeds.

These findings are difficult to reconcile with the standard two state model of hippocampal function (Buzsaki, 1989, Hasselmo, 1999). Rather, we found that the patterns of activity we examined were smoothly modulated over a range of movement speeds. We propose that the traditional two states reflect extrema of a continuum in which the patterns of activity expressed in CA1 reflect the strength of the CA3-CA1 pathway. Traditionally, studies of place cell activity have set a speed threshold and combined all speeds above that threshold together for analysis. Our findings demonstrate that there are significant differences in the prevalence of CA3 and EC driven patterns in CA1 at speeds that traditionally would have been combined. Similarly, the level of correlated activity in CA1 decreases with increasing speed, reflecting these different patterns of activity, suggesting that variations in the input to CA1 as a function

of speed has the potential to alter the way CA1 activity influences downstream structures. These fast alterations in circuit activity suggest that a complete understanding of hippocampal activity and its influence on target structures will require knowledge of the specific recent history of neural activity and ongoing behavior.

Our findings also provide new insight into how and when CA3 spiking can influence activity in CA1 and how those changes manifest in correlated activity in the CA1 network. Our findings suggest that the strength of the CA3 – CA1 Schaffer collateral pathway plays a central role in regulating the prevalence of slow gamma, ripples and correlated spiking in CA1. Further, during learning there is a large increase in the prevalence of CA3 driven patterns in CA1 at low speeds and an increase in the prevalence of EC-associated fast gamma at high speeds. These results suggest that new experiences result in greater drive to CA1, providing a potential explanation for the higher firing rates seen in CA1 during new experiences (Nitz and McNaughton, 2004, Csicsvari et al., 2007, Karlsson and Frank, 2008).

Head movement speed provides an experimentally measurable parameter that effectively characterizes the degree to which CA1 activity is driven by CA3. As low and intermediate values of movement speed were only weakly correlated with speed along the axis of the track, and as these low and intermediate speeds were more prevalent in novel environments, our results indicate that measuring movement speed captures important elements of behavior associated with learning. Movement speed is a behavioral parameter, however, and thus cannot directly affect the strength of specific hippocampal pathways. Nonetheless, differences in speed captured as much as 50% of the variance in fEPSP slope, indicating that the causal factor(s) must be tightly correlated with speed. Further, speed modulation was strongest in novel environments, indicating that the causal factor(s) should be enhanced during learning. Cholinergic

modulation of the hippocampal circuit is a likely candidate. First, acetylcholine has been shown *in vitro* to differentially suppress both the SC and EC layer III input to CA1 in a dose dependent manner, with significantly greater suppression of the SC pathway (Hasselmo and Schnell, 1994). This difference between the effect of cholinergic tone on SC and EC inputs to CA1 could explain the relative increase in EC-associated fast gamma power seen with increasing speed. Second, The firing rate of neurons recorded *in vivo* from the medial septum, which sends cholinergic projections to the hippocampus (Amaral and Witter, 1995), increases with movement speed (King et al., 1998). Third, acetylcholine levels are higher in novel, as compared to familiar environments (Giovannini et al., 2001). Fourth, cholinergic modulation is also involved in regulating the hippocampal theta rhythm (Lee et al., 1994), consistent with the strong relationship between movement speed and theta power. Finally, the timescale of action of acetylcholine may also be consistent with the rapid modulation we seen (Parikh et al., 2007). Taken together, these studies suggest that the cholinergic tone in the hippocampus increases with movement speed and that cholinergic modulation could account for the observed change in the influence of CA3 on CA1.

The speed related changes in ensemble activity we found were present in both novel and familiar environments, indicating that speed-related changes in correlations are a consistent feature of the hippocampal code. Previous studies have for the most part assumed a two state model of CA1 activity and focused on presence of coordinated activity in sets hippocampal place cells active either during movement (Harris et al., 2003, Dragoi and Buzsaki, 2006, Kelemen and Fenton, 2010, Singer et al., 2010) or during stillness (Kudrimoti et al., 1999, Foster and Wilson, 2006, Karlsson and Frank, 2009). Our results suggest that the expression of these ensembles reflects a common factor: the relative strength of CA3 input to CA1. Further, the consistent and substantial

decrease in residual correlations seen with higher movement speeds suggests that ensembles are not present or absent, but rather are expressed to a greater or lesser extent on a moment-by-moment basis.

Why might coordinated activity in CA1 be expressed dynamically? Correlations among neurons can be useful for driving plasticity or expressing specific stored representations, but correlations can also reduce the overall information content of a neural code (Averbeck et al., 2006). Thus, correlations in place cell activity during exploration could signal specific associations related to a place, but the expression of the coordination makes the spatial information itself less robust. In a novel environment, the increased correlated activity seen both during ripples and in the context of place fields is well suited to promote the plastic changes involved in building a representation of the environment. The more de-correlated place field activity present at high speeds provides an accurate and informative representation of the animal's current location to downstream structures. In more familiar environments, the highly correlated activity seen at low speeds is well suited to support memory retrieval. This notion is consistent with observation that animals tend to slow down at decision points where memory is required (Johnson and Redish, 2007) and suggests that memory retrieval will be facilitated at lower movement speeds.

We hypothesize that the continuous modulation of the influence of CA3 on CA1 allows the hippocampus to subserve different functions at different times. At slow speeds CA3 input is strongest. At these times, we observe prominent ripple oscillations, which are thought to support memory consolidation via replay of previously stored associations (Girardeau et al., 2009, Carr et al., 2011). Intriguingly, the correlated place cell activity we observed at slow speeds also reflects the co-activation of neural ensembles on timescales that are thought to be well suited for driving synaptic plasticity in downstream

structures (Hebb, 1949). Taken together, these results suggest that when CA3 input is strongest, CA1 activity reflects associations stored in CA3 which may promote learning at the CA3-CA1 synapse and in distributed neo-cortical circuits and enable retrieval in these networks. As animals move more quickly, activity in CA1 shifts from representing primarily stored associations towards faithful representations of location. Thus movement speed and novelty are critical variables in understanding the smooth dynamics of the CA3-CA1 pathway and the structure the hippocampal output.

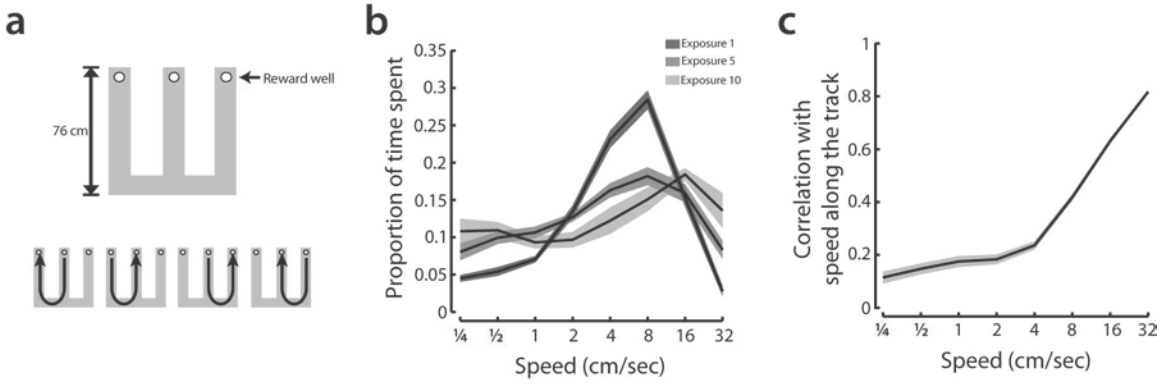

Figure 1 | Movement speed varies on a rapid timescale and new experiences lead to increased exploration. **(a, top)** Rats were introduced to a novel W shaped environment where they learned to perform a spatial alternation task over multiple 15 minute exposures. (bottom) Animals were rewarded at the ends of each arm when they performed the correct sequence of trajectories: from center arm to left to center to right to center… **(b)** The head movement speed distributions for exposures 1, 5, and 10 to an initially novel W-track. Means are shown with solid lines and standard errors with shaded regions. **(c)** Correlation between speed, measured in two dimensions, and linear speed along the axis of the track. Lower correlations at intermediate speeds are consistent with exploratory behavior.

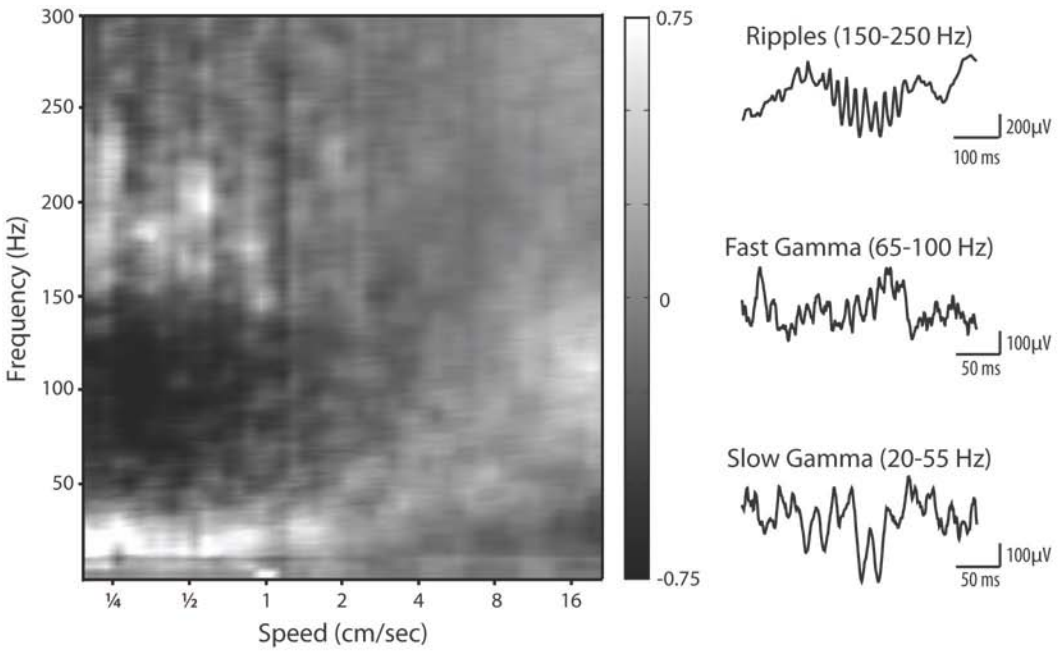

Figure 2 | The spectrum of rhythmic local field potential activity in area CA1 is smoothly modulated by behavior. **(left)** Example spectrogram across speeds. Power in each frequency is shown as a z-score relative to the mean power across speeds. **(right)** Three known and physiologically relevant rhythms, the ripple oscillation (150-250 Hz), fast gamma (65-100 Hz), and slow gamma (25-55 Hz).

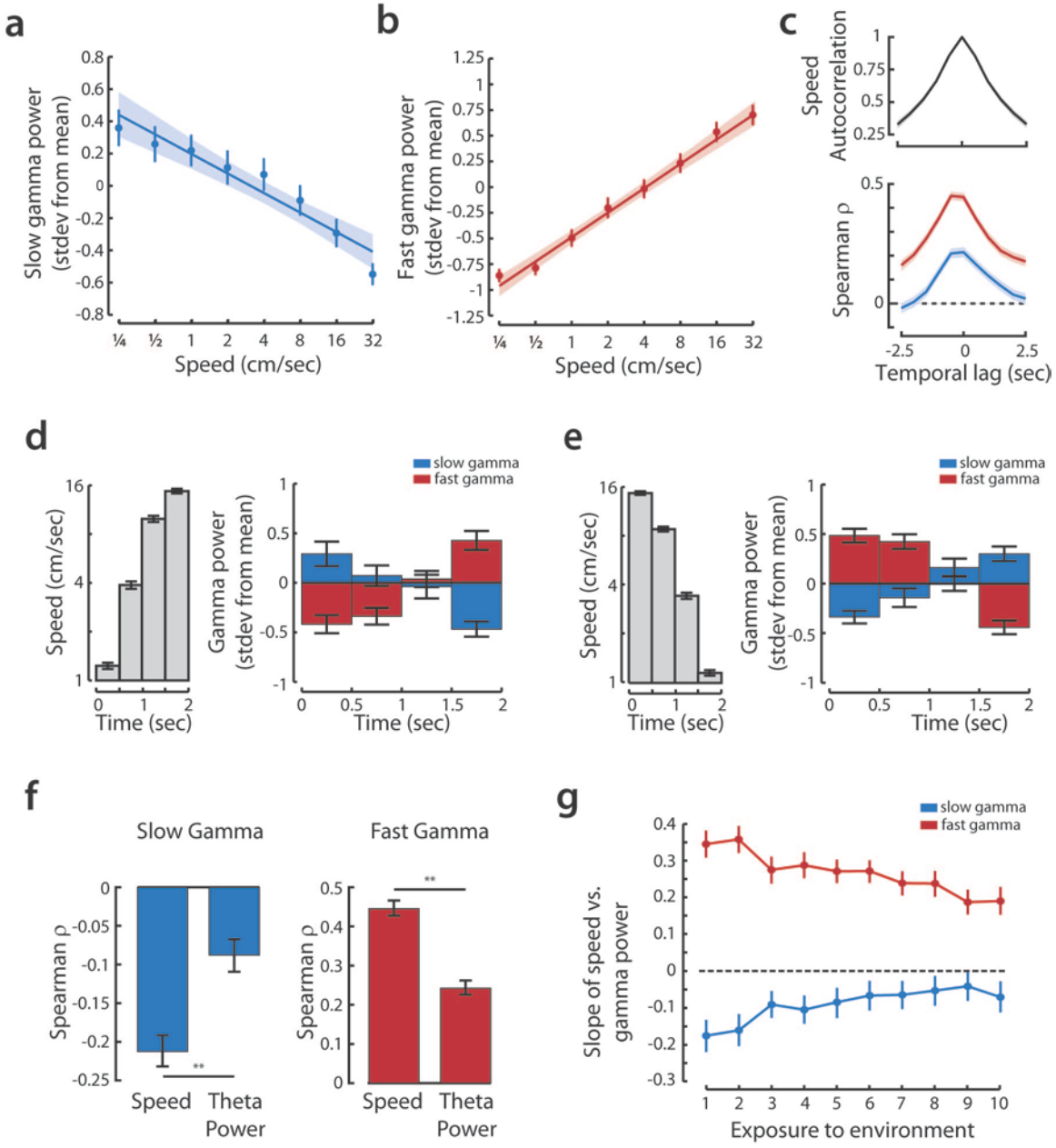

Figure 3 | Slow and fast gamma oscillations in CA1 are rapidly modulated by speed. **(a)** Population data showing normalized power of slow gamma vs. speed. Points represent binned means with standard error using logarithmically spaced bin centers; line represents linear regression of underlying data with 95% confidence intervals. **(b)** Population data showing normalized power of fast gamma oscillations vs. speed. Points and line as in **(a)**. **(c,top)** The autocorrelation of speed (shown with bootstrap 95% confidence interval) during the first exposure shows a rapid fall-off of on the timescale of ~1 second. **(bottom)** Both fast and slow gamma power is most modulated by the animal's speed measured within a second of the gamma power estimate, implying a rapid timescale of modulation.

Figure 3 (continued) | Shown are the Spearman correlation and bootstrap 95% confidence interval of fast (red) and slow (blue) gamma power with log(speed) for offsets in speed measurement ranging from -2.5 to 2.5 s relative to the 0.5 s window used to estimate gamma power. **(d)** Rapid and opposing changes in the power of slow and fast gamma are apparent in 2 second windows over which rats' speed increase from less than 2 cm/s to more than 10 cm/s. **(left)** Increasing mean speed (with standard errors) in 0.5 s windows corresponding to the isolated increasing speed incidents. **(right)** Mean slow gamma power (blue bars with standard errors) decreases significantly, while fast gamma simultaneously increases significantly (red bars) over the course of the two second increasing speed events. **(e)** Same analysis as **(d)** but for 2 s windows when speed decreased from more than 10 cm/s to less than 2 cm/s. Periods of decreasing speed are marked by an increase in slow gamma power (blue bars) and a concomitant decrease in fast gamma power (red bars). **(f)** Speed is a better predictor of slow and fast gamma power than theta power. Comparison of Spearman correlation log(speed) or theta power with **(left)** slow gamma power and **(right) fast** gamma power. Depicted are correlations with bootstrap 95% confidence intervals. **(g)** Slope of the linear regression of slow and fast gamma power vs. speed plotted across exposures to the environment. Points show slope with 95% confidence bounds by bootstrap. **p<0.01.

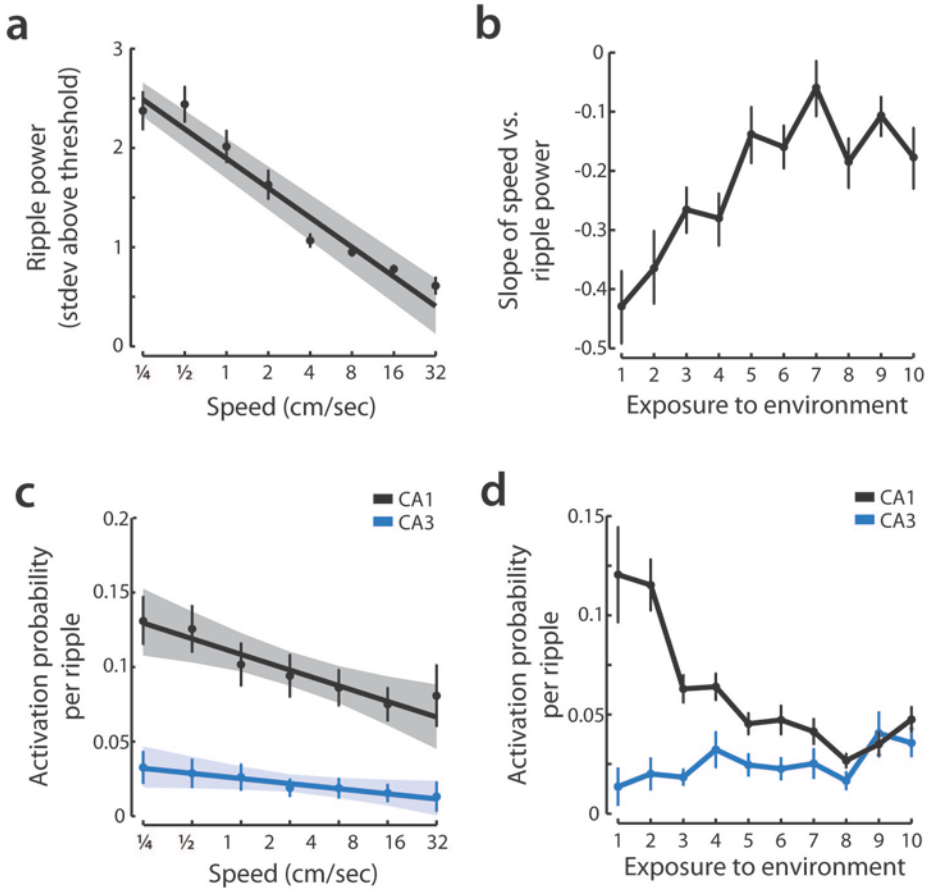

Figure 4 | Ripple oscillations and CA1 spiking during ripples reflects the dynamics of CA3 input to CA1. **(a)** Normalized ripple power (measured from threshold for detecting ripples) vs. speed. For clarity, normalized ripple power is displayed both as binned averages (binned means and standard error using logarithmically spaced bin centers) and regression to the underlying data (slope with 95% confidence range by bootstrap). **(b)** Changes in speed modulation over exposures to the environment. Points represent means +/- 95% confidence bounds by bootstrap. **(c)** Activation probability during each ripple for CA1 and CA3 cells. For clarity, activation probability is displayed both as binned averages (binned mean and standard error using logarithmically spaced speed bins) and best fit line (linear regression of the underlying data with 95% confidence intervals). **(d)** Mean activation probability for CA1 and CA3 neurons across exposures to the environment. Points show mean probability with 95% confidence bounds by bootstrap.

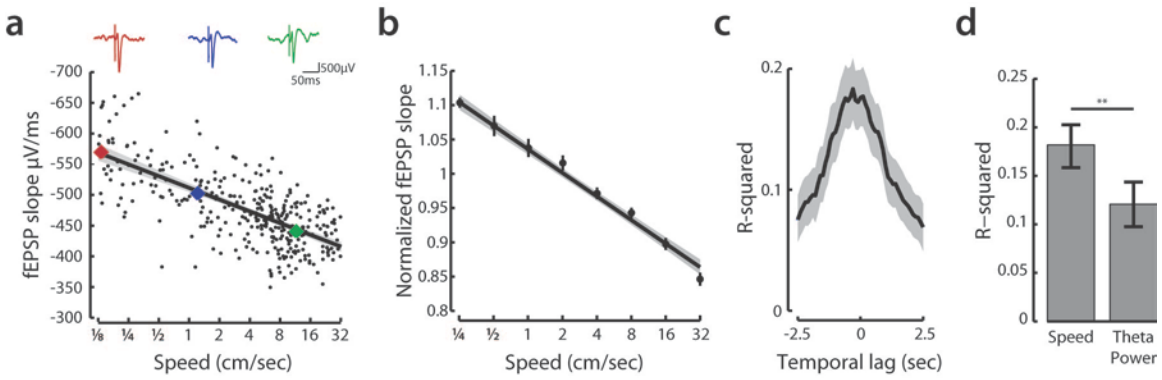

Figure 5 | Rapid modulation of the Schaffer collateral pathway as a function of movement speed. **(a)** Modulation of EPSPs evoked in area CA1 by stimulation of the SC pathway as a function of speed. Colored points represent the measured slopes of the individual fEPSP example shown at top. The regression of fEPSP slope against log(speed) is shown with a 95% confidence interval estimated by bootstrap. **(b)** The modulation of the SC pathway by speed is seen in fEPSP measurements normalized and pooled across animals/recording sessions. Normalized measurements are displayed both as binned averages (binned mean and standard error using bin centers on horizontal axis) and a regression line with bootstrapped 95% confidence interval. **(c)** The strength of evoked fEPSPs is most strongly related to the speed measured at the time of stimulation. Depicted are mean and bootstrapped 95% confidence interval of the R^2 for regressions of normalized fEPSP size to log(offset speed). **(d)** Speed is a better predictor of evoked fEPSP size than theta_power. Compared are R^2 for log(speed) vs fEPSP slope and for theta power vs fEPSP slope. Error bars show 95% confidence interval estimated by bootstrap. **p<0.001.

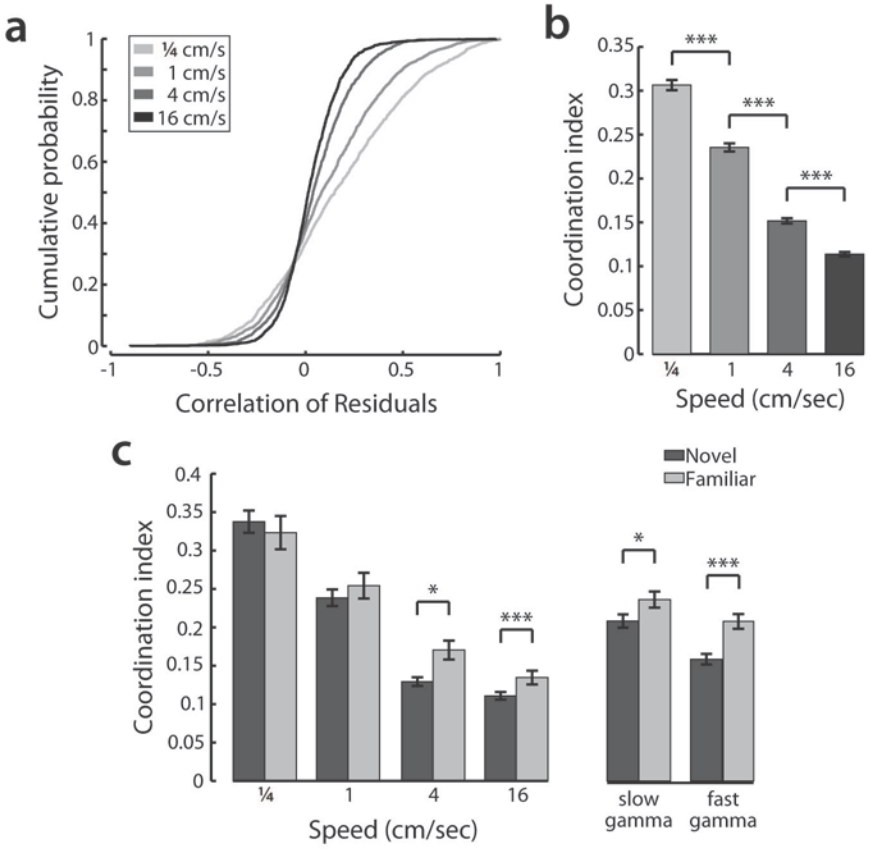

Figure 6 | Correlated activity in CA1 reflects the influence of the associational CA3 network. **(a)** Cumulative distribution of residual correlation of cell pairs across speed bins. **(b)** Coordination index for cell pairs across speeds. **(c)** Coordination index for within day novel vs. familiar comparison for different speeds (right) and, for the same data, for periods of slow or fast gamma. Bars show mean and standard error. * $p < 0.05$; *** $p < 10^{-5}$.

Supplemental Figures

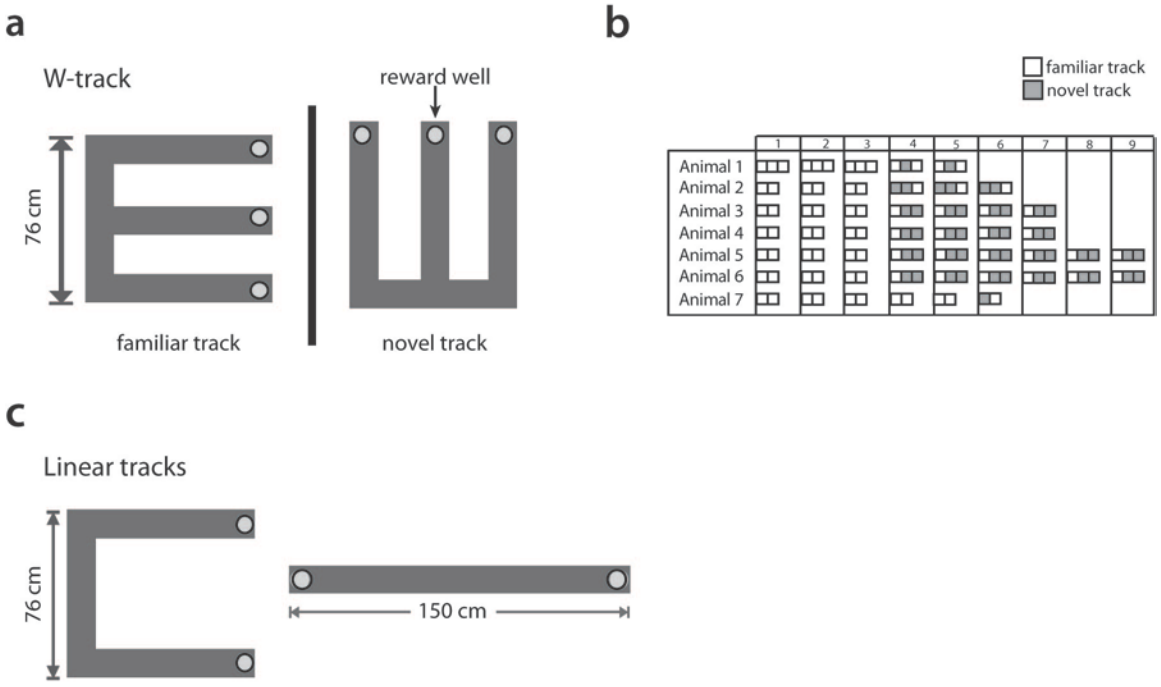

Figure S1 | Behavioral tasks. We used two distinct types of behavioral paradigms. Animals either performed a hippocampally dependent spatial alternation task or a simple linear task. **(a)** Animals learned to perform a spatial alternation task in two geometrically identical, but visually distinct W-shaped environments. Animals were rewarded for performing the alternation sequence (center, left, center, right, center, ...). **(b)** The recording schedule for each animal, organized by experiment day. White squares indicate a 15 minute run on the familiar track. Grey squares represent a 15 minute run on the more novel track. All run sessions were separated by 20 minute rest sessions in a familiar sleep box. Data from the familiar track was used for all analyses except for within day comparisons to study the effect of novelty. Comparisons were made between the first session on the second track and the familiar session immediately preceding it for animals 1, 3, 4, and 5. Animal 6 was not included for within day comparisons due to electrical artifacts in LFP recorded in the novel environment. **(c)** Experiments which related the size of fEPSPs to animal speed were performed in straight or U-shaped linear tracks (n = 4) and in the W-shaped alternation task (n = 3).

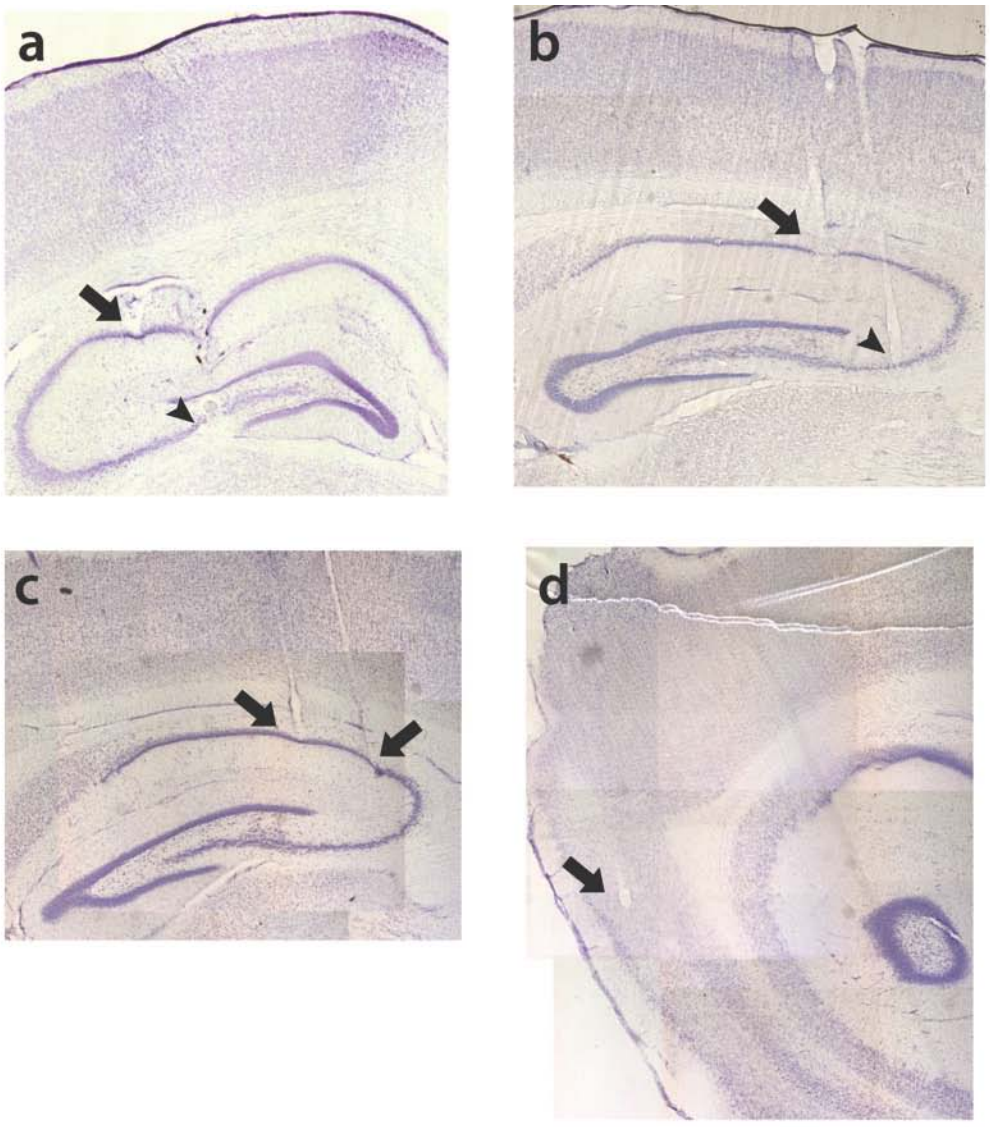

Figure S2 | Examples of tetrode placement. **(a)** Coronal section showing example of tetrode placement in CA1 (arrow) and CA3 (arrowhead) from stimulation experiment. **(b)** Sagital section showing example of tetrode placement in CA1 (arrow) and CA3 (arrowhead) from recording only experiment. **(c-d)** Sagital sections from recordings targeting CA1 and entorhinal cortex showing example of **(c)** two tetrode targeting CA1 (arrow) and **(d)** a lesion from one tetrode targeting layer 3 of medial entorhinal cortex (arrow). Images are composed from multiple adjacent photos.

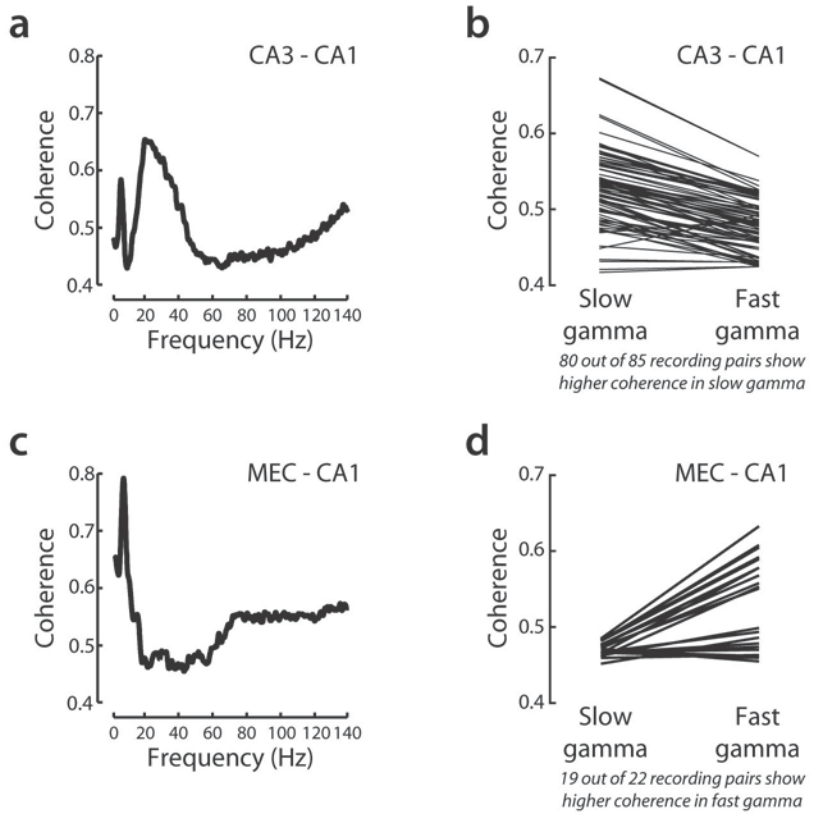

Figure S3 | Gamma oscillations in area CA1. **(a-d)** CA1 is more coherent with CA3 in slow gamma range and more coherent with layer 3 of the medial entorhinal cortex in fast gamma range. **(a)** Coherence plot for a representative pair of CA3-CA1 recordings. There is a pronounced peak in the slow gamma range (25 - 55 Hz). **(b)** Slow gamma coherence was greater than fast gamma coherence for 80 out of 85 pairs of CA3-CA1 recordings (z-test for proportions, $p < 10^{-5}$; n = 5 animals). **(c)** Coherence plot for a representative pair of layer 3 MEC-CA1 recordings. There is a noticeable increase in the fast gamma range (~70-130Hz). **(d)** Fast gamma corherence was greater than slow gamma coherence for 19 out of 22 pairs of MEC-CA1 recordings (z-test for proportions, $p<10^{-5}$; n = 2 animals).

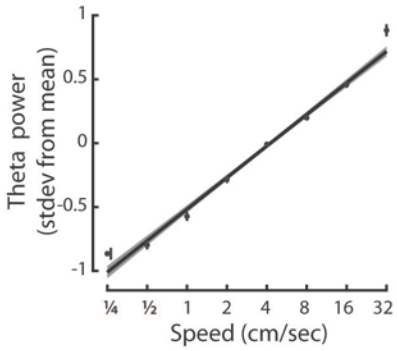

Figure S4 | Theta power is smoothly modulated by animal speed. Correlation between theta power and log(speed). The graph shows population data of normalized power of theta oscillation (7-9 Hz) vs. speed, both measured over 0.5 s windows. Points represent binned means with standard error; line shows linear regression of underlying data with 95% confidence intervals.

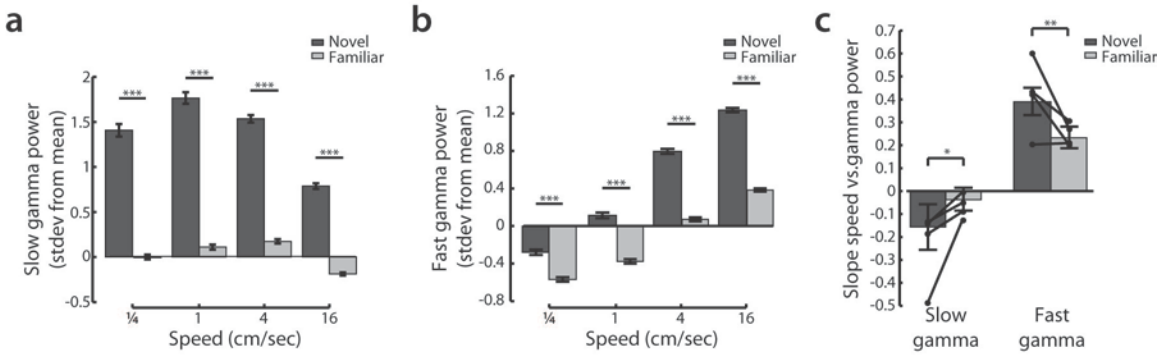

Figure S5 | Novelty enhances the depth of modulation as well as the amplitude of gamma oscillations. On days in which a second novel environment was experienced immediately following the first, more familiar environment (n = 4; see methods and Figure S1), the effect of novelty on slow **(a)** and fast **(b)** gamma power could be directly measured. Shown are the mean binned gamma power in the novel (black) and familiar (gray) environments. Slow and fast gamma power are significantly increased in the novel as compared to the familiar environment for all speeds (rank sum test between novel and familiar session; slow gamma, $p < 10^{-5}$ for all speed bins; fast gamma $p < 10^{-5}$ for all speed bins). **(c)** The depth of gamma modulation by speed (more negative slope for slow gamma and more positive slope for fast gamma) is larger in a novel as compared to a familiar environment. Bars show grouped data, means with 95% confidence intervals, thin lines show change in slope for individual animals (bootstrap estimate of slope, novel slope vs. familiar slope; slow gamma $p<0.01$ for group, $p < 0.05$ for individuals; fast gamma $p<0.001$ for group, $p<0.05$ for 3 out of 4 individual animals, one animal n.s.). *$p<0.05$; **$p<0.001$; ***$p<10^{-5}$.

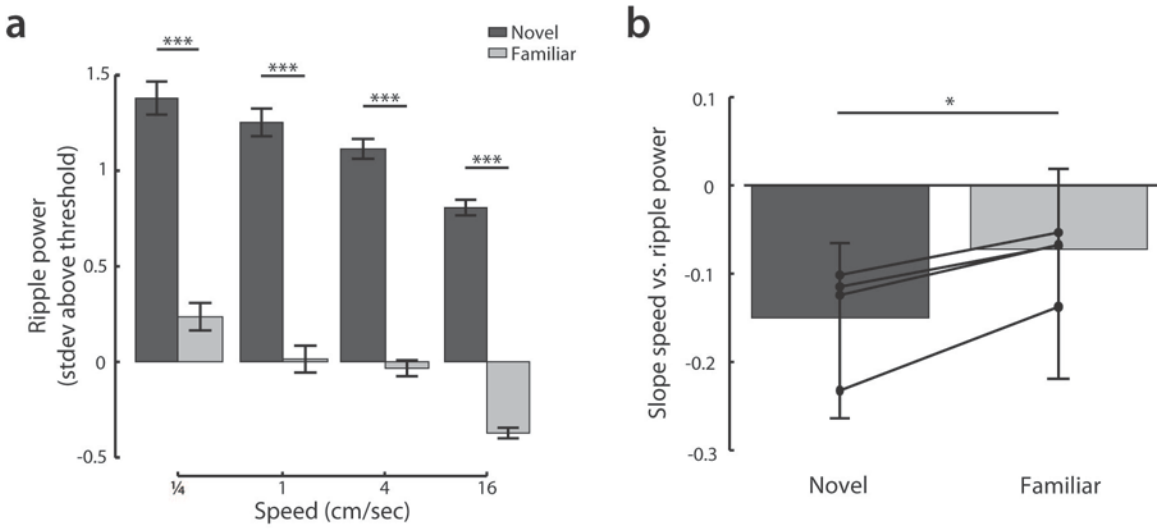

Figure S6 | Novelty enhances the depth of modulation as well as the amplitude of ripple oscillations. **(a)** On days in which a second novel environment was experienced immediately following the first, more familiar environment (n = 4; see methods and Figure S1), the effect of novelty on ripple power could be directly measured. Shown are the mean binned ripple power in the novel (black) and familiar (gray) environments. Ripple power is significantly increased in the novel as compared to the familiar environment for all speeds (rank sum test between novel and familiar session, $p < 10^{-5}$ for all speed bins). **(b)** The depth of ripple power modulation by speed is larger in a novel as compared to a familiar environment. For all animals where it was possible to measure within day changes, we find that there was a significant increase in the depth of modulation (more negative slope) in the novel as compared to more familiar environment. Bars show grouped data, means with 95% confidence intervals, thin lines show change in slope for individual animals (bootstrap estimate of slope, novel slope vs. familiar slope, $p<0.05$ for group, $p<0.05$ for individual animals). *$p<0.05$; ***$p<10^{-5}$.

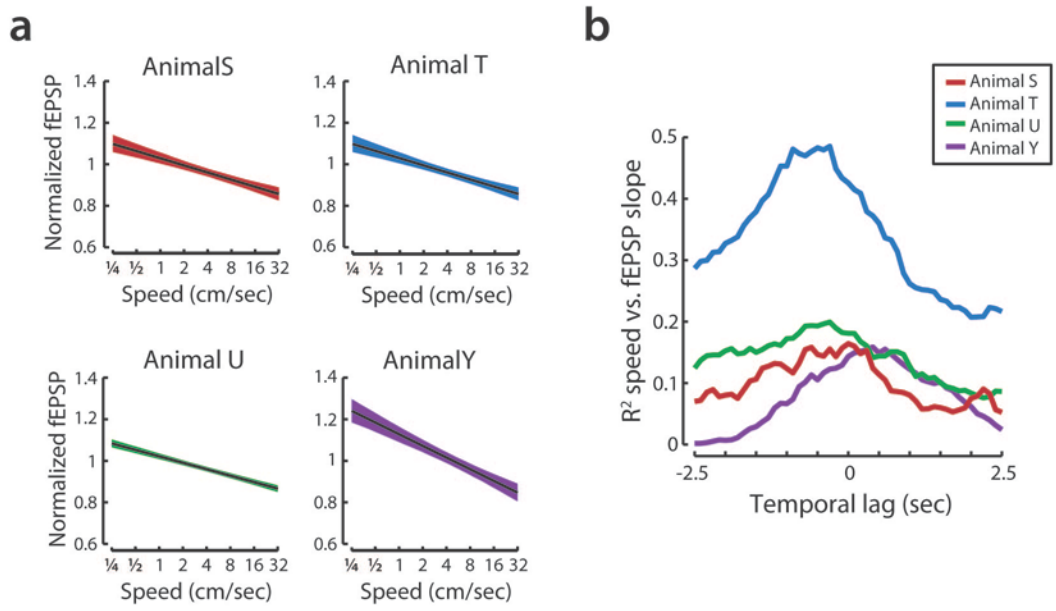

Figure S7 | Evoked fEPSP slopes by animal. In this study we combined measurements of fEPSPs recorded in 4 animals and a total of 31 behavioral epochs. As described in the text, we normalized responses in each epoch to account for variability between animals and epochs. While the evoked responses in some animals were small, resulting in a small signal to noise ratio, all animals exhibit the trends shown in Figure 5. **(a)** The relationship between log(speed) and normalized fEPSP slopes recorded in CA1 in response to optical and electrical stimulation is observed in all animals. Shown are regression lines and 95% confidence intervals for each animal (number of responses and mean fEPSP slope across all epochs by animal: S – 361, 311 μV/ms; T – 1022, 598 μV/ms; U – 875, 370 μV/ms; Y – 515, 291 μV/ms). Note negative slope in all animals (bootstrap regression log(speed) vs. normalized fEPSP slope; p's < 0.01 for all animals). **(b)** For all animals with significant modulation of fEPSP strength by speed, the delay between speed and fEPSP produced a maximal R^2 statistic at short temporal offsets indicating moment-by-moment modulation of the synapse. In all cases an examination of the confidence bounds indicated that the peak R2 was not different than zero (not shown).

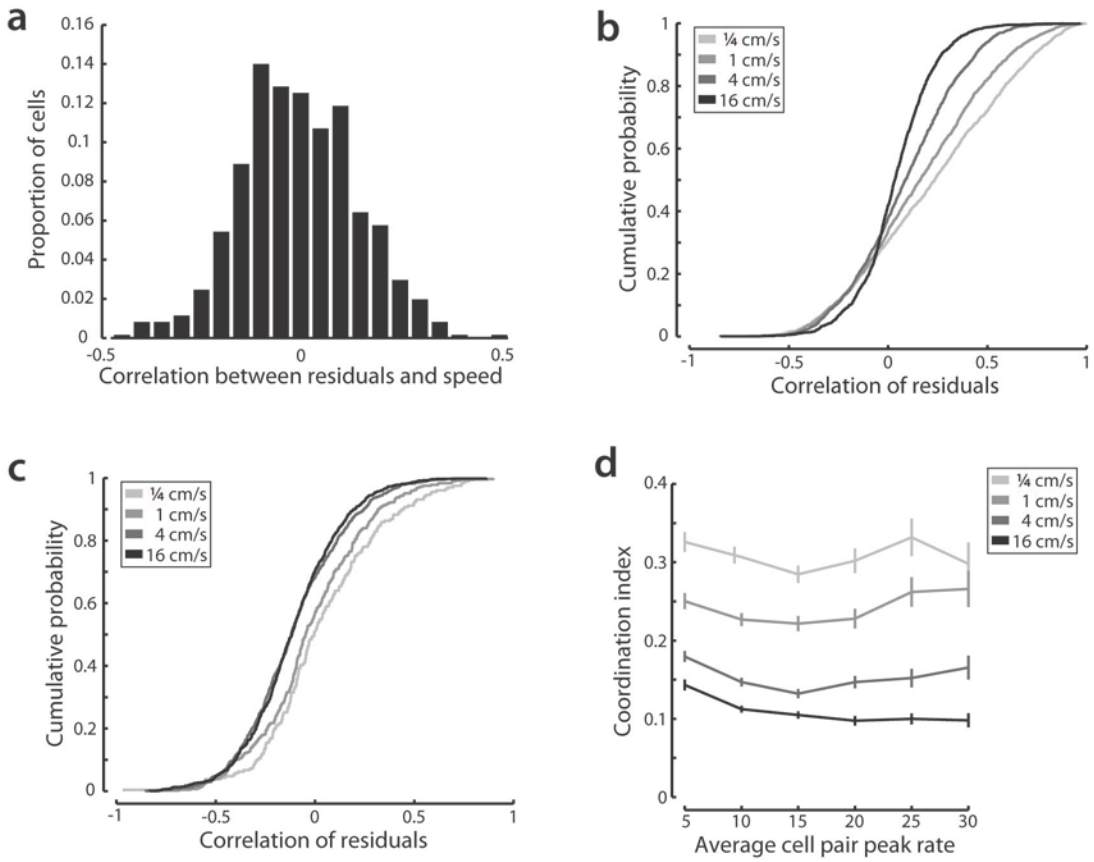

Figure S8 | Modulation of residual correlation as a function of speed cannot be explained by choice of parameters. **(a)** While the correlation of residuals varies with speed, this cannot be explained by covariation between the residuals themselves and speed. Shown is a histogram of the Spearman correlation between the residuals for individual cells and movement speed. Note that the correlation between residuals and speed is centered on zero (ttest on correlation values, $p > 0.3$). **(b)** The relationship between residual correlation and speed is present when we use time bins consistent with a theta cycle (125ms; kstest, $p<10^{-5}$ for all pairs). **(c)** The relationship between residual correlation and speed is present when limiting the measurement to within place fields (both cells min occupancy normalize rate > 1 Hz; kstest, p<10-5 for 1/4 vs. 4 cm/sec, 1/4 vs. 16 cm/sec, 1 vs. 4 cm/sec, and 1 vs. 16 cm/sec; no significant difference between 1/4 and 1 cm/sec or 4 and 16cm/sec). **(d)** The relationship between residual correlation and speed is present regardless of peak rate. Shown are the mean and standard error for the average cell pair peak rate for each speed bin. For every peak rate, speed modulated the residual correlation (2 way ANOVA, post-hoc tests, main effect of speed (F=311.5, p<10-5); no interaction between rate and speed F = 0.91, p>0.5). The same was true whether we examined the average peak rate between cell pairs (shown), the maximum peak rate between cell pairs, or the minimum peak rate between cell pairs (data not shown).

Methods

Data Acquisition

11 male Long Evans rats weighing between 400-600 grams were used. Neuronal activity was recorded in 7 rats with 30 independently movable tetrodes assembled in two bundles targeting dorsal hippocampal region CA1 and dorsal CA3 (n=4)(Karlsson and Frank, 2008), CA1 and EC (n=2; two 15 tetrode groups centered at -3.6mm AP, 2.2mm ML for hippocampal targets and 9.1mm AP, 5.6mm ML at a 10° angle in the sagital plane for medial entorhinal targets, coordinates relative to bregma), or CA1, CA3 and EC (n=1; same coordinates as CA1 and EC implantation). Analyses of data from the CA1-CA3 animals has been reported previously(Karlsson and Frank, 2008, 2009). On the days following surgery, hippocampal tetrodes were advanced to the cell layers and entorhinal tetrodes were advanced through primary visual cortex until characteristic EEG patterns were observed. All spiking activity was recorded relative to a reference tetrode located in the corpus callosum. Local field potentials were recorded relative to ground. Tetrode positions were adjusted after daily recording sessions for all tetrodes that had poor unit recordings. Recording was initiated when EEG characteristics (sharp wave polarity, theta modulation) and neural firing patterns indicated that the target regions had been reached. On rare occasions, some tetrodes were moved before recording sessions but never within 4 h of recording.

In a second set of experiments, electrically evoked responses were recorded in 4 male Long Evans. Movable 10 kΩ tungsten or platinum iridium bipolar stimulating electrodes (MicroProbes for Life Science, Gaithersburg, MD) were lowered into either the ventral hippocampal commissure (n=3; coordinates relative to bregma: -1.3 mm AP, +1.0 ML) or contralateral CA3 to stimulate the Schaffer collateral pathway (coordinates relative to bregma: -3.6 mm AP, -3.6 mm ML). Either a multi-tetrode array (n=2; coordinates

relative to bregma: -3.6 mm AP, -2.2 mm ML) or a 16-channel linear array silicon probe (NeuroNexus Technologies, Ann Arbor, MI; n =2; coordinates relative to bregma: -3.6mm AP, -3.6mm ML (n=1) or -2.2mm ML (n=1)) was implanted above the dorsal hippocampus.

The depth of electrical stimulation electrodes was set to maximize evoked responses. Recording was initiated when EEG characteristics indicated that movable tetrodes had reached their target regions and animals had fully recovered from surgery. For all electrical stimulation experiments the level of current in the 0.2 ms biphasic pulse (A-M Systems, Sequim, WA) was set to evoke easily measurable fEPSPs in area CA1, typically halfway between threshold and maximum response, and between 50-250 µA. The level of current was always held constant across multiple sessions recorded in a single day.

Recording only experiments

Prior to implantation, animals were food deprived to 85-90% of their baseline weight and pretrained in a separate room to run back and forth on a raised track for liquid food reward (evaporated milk) at each end. Animals were exposed sequentially to two physically different W-shaped environments (76 x 76 cm with 7cm wide track sections) and during intervening sessions in a high walled rest box (20 minute rest periods, floor 25 x 34 cm; walls, 50 cm tall)(Karlsson and Frank, 2008). Each rat was exposed to the first initially novel W-track and after either three days (n = 6) or five days (n = 1) of two run sessions per day, rats were introduced to a second W-track. The two W-tracks were oriented at 90 degrees with respect to one another and were separated by a high barrier so that the rat had access to largely distinct sets of visual cues. Both environments had one reward site at the endpoint of each arm and animals were rewarded for performing a

continuous alternation task(Frank et al., 2000). Rapid learning of this task requires an intact hippocampus(Kim and Frank, 2009). Animals completed two or three 15-min run sessions per day (Figure S1).

Stimulation Experiments

Prior to implantation, animals were food deprived to 85-90% of their baseline weight and trained to run back and forth on a raised track for liquid food reward (sweetened soy or evaporated milk) at each end. We used two different track designs, a linear track (either straight or U-shaped; 4 animals, 22 epochs) with food wells at each end and a W-shaped maze (described above; 3 animals, 9 epochs). All pretraining was done in the recording room such that pretraining familiarized animals with both the tracks and the spatial context. We recorded one to three run sessions each day interspersed by 20 minute periods in which the animal rested in a small enclosed box. To measure synaptic strength as rats behaved, we triggered electrical pulses at 0.05 – 0.1 Hz for several minutes at a time. Thus, for each animal and day of behavior, we gathered a set of field and spiking responses in area CA1 (31 data sets, minimum 46 and maximum 193 pulses).

Following the conclusion of the experiments we made microlesions through each electrode tip to mark recording locations (30 μA for 3 sec). After receiving an overdose of Euthanasol, animals were perfused intracardially with isotonic sucrose and 4% PFA. The brains were stored in PFA, frozen, cut either coronally or sagitally at 50 μm sections, and stained with cresyl violet. Exact reconstructions were not available for one CA1-EC recording animal, so we verified the locations of tetrodes targeted to the EC using theta coherence and theta polarity relative to CA1 as well as the absence of ripples in the LFP at the time of CA1 ripples(Mizuseki et al., 2009). EC tetrodes were included for analysis

only if the theta and ripple related activity was consistent with layer 3 recordings. We also verified that results from these tetrodes were consistent with results from tetrodes with histologically verified recording locations.

Data were collected using the NSpike data acquisition system (L.M.F. and J. MacArthur, Harvard Instrumentation Design Laboratory). During recording sessions, we recorded both local field potentials (filtered 0.5—400 Hz and sampled at 1500 Hz) and threshold-crossing spike snippets (40 samples at 30 kHz, filtered 300-3000 Hz or 300-6000 Hz). An infrared light emitting diode array with a large and a small cluster of diodes was attached to the preamps during recording. Following recording, the rat's position on the track was reconstructed using a semi-automated analysis of digital video of the experiment. The position of the front and back tracking diodes extracted from the video were first smoothed using a nonlinear method(Hen et al., 2004). We computed speed by taking the difference in position and then smoothing using a Gaussian kernel with standard deviation 0.5 s and a total length of 6 seconds.

Single neuron data were clustered using custom software (MatClust, M. Karlsson) as described previously(Karlsson and Frank, 2008). We used standard waveform and mean rate criteria to separate putative excitatory pyramidal cells from putative inhibitory fast spiking cells(Fox and Ranck, 1981, Frank et al., 2001).

For measuring evoked responses from the SC pathway the best measurements are obtained below *stratum pyramidae*, in which a large fEPSP can be recorded with a peak amplitude at approximately 8-12 ms. In recordings where multiple tetrodes were available, we chose the tetrode with the largest consistent response. By recording below the cell layer, we attempted to avoid contamination from population spikes. For the silicon probe recordings of stimulation of the SC pathways, we measured the fEPSPs

from recording sites near the *stratum radiatum* current sink revealed via current-source density analysis. The fEPSP measurements were highly variable in size across days and between animals. Thus, in order to combine across different recording days, we needed to normalize our data. For ease of comparison to other work, we chose to use a multiplicative normalization, scaling each fEPSP measurement by the average across all evoked responses during a given session. For the analysis of the effect of environmental novelty, we normalized fEPSP measurements in both sessions by the average from the familiar session. For regression analyses we eliminated points with a speed below 1/8 cm/sec ensure robust linear fits in relation to log(speed).

Analysis

Speed spectrogram

A windowed power spectrum was computed for a tetrode located in the CA1 cell layer using the multi-taper method from the Chronux toolbox. Multi-taper estimates of the power spectrum were obtained for 0.5 second non-overlapping windows and a z-score was computed for each frequency band. Thus for each 0.5 second bin, we obtained a normalized measure of power for each frequency band in units of standard deviations from the mean. We assigned each of these 0.5 second normalized power spectrum to a logarithmically spaced speed bin and then plotted the mean power for each speed bin.

Identifying slow and fast gamma

For gamma analyses, we defined slow and fast gamma bandwidths and gamma events as described previously(Colgin et al., 2009). Briefly, for each animal cross-frequency coherence was computed on the local EEG to determine slow and fast gamma bands. A lower limit was set to 20 Hz and an upper limit was set to 140 Hz to exclude theta harmonic and contamination by spikes. In 6 out of 7 cases, there was a clear separation

between slow and fast gamma. One animal was excluded from all gamma analyses due to large 60Hz noise which precluded adequate separation of slow and fast gamma bands.

Gamma Oscillation Analyses.

A windowed power spectrum was computed for each tetrode located in the CA1 cell layer using the multi-taper method from the Chronux toolbox. Multi-taper estimates of the power spectrum were obtained for 0.5 second non-overlapping windows, a z-score was computed for each frequency band and the power spectrum was averaged across all CA1 tetrodes. Thus for each 0.5 second bin, we obtained a normalized measure of slow and fast gamma power in units of standard deviations from the mean. For regression analyses we eliminated points with a speed below 1/8 cm/sec ensure robust linear fits in relation to log(speed). As the distribution of the residuals was non-gaussian, we used a bootstrap resampling method to determine the significance of the linear regression, resampling data to ensure equal sampling across four logarithmically spaced speed bins with centers at [1/4, 1, 4, 16] cm/s. To evaluate the temporal specificity of speed modulation, we measured the Spearman correlation (a non-parametric measure) of normalized gamma power (in 0.5 s bins as described above) with log(speed) in the concurrent and adjacent time bins. We used a bootstrap to estimate the mean and 95% confidence interval of the correlation. To investigate how the depth of modulation changed across exposures, we used a bootstrap estimate of slope for each exposure, while resampling to ensure equal sampling across different speeds. To test for significant changes in slope over days, we used a permutation test to test against the null hypothesis. To measure the within day differences in gamma power between novel and familiar experiences, we normalized all data to the power spectrum from the familiar session. After binning the data into logarithmically spaced speed bins we used a rank

sum test to measure the difference in normalized gamma power between comparable speeds in the novel and familiar track. To measure the within day differences in the depth of modulation between novel and familiar experience we computed 1000 bootstrap estimates of the slope to ensure equal sampling across animals and across different behaviors.

Coherence Analyses.

Coherence between CA1 and either CA3 or layer 3 of entorhinal cortex was computed for all CA1-CA3 or CA1-EC tetrode pairs. Coherence was computed between tetrode pairs using the multi-taper method from the Chronux toolbox. Multi-taper estimates of the cross-spectra were obtained for 10 second non-overlapping windows, and then all of the estimates were averaged in order to calculate the coherence. The mean coherence in the slow and fast gamma band were computed for all tetrode-pairs.

Theta Power

To compare whether speed or the strength of the theta rhythm is more predictive, we extracted theta power from our recordings. When available (n=2), we measured the theta power using recordings in the hippocampal fissure. Alternatively, we used the callosal reference electrodes (n=5), or if these were not available, electrodes in area CA3 (n=2). We measured theta power by first 7 – 9 Hz bandpass filtering (FIR filter, 6, 10 Hz stopband) the recorded LFP. Our measure of theta power was the magnitude of the Hilbert transform of the filtered LFP. For the analysis of the modulation of gamma power by theta power, we used the theta power averaged over the 0.5s spectral estimation window. For the analysis of the modulation of evoked fEPSP slope by theta power, we used the average theta power measured in the second prior to stimulation. To

combine theta power across pooled data sets we computed a z-score of theta power across each epoch.

Ripple Oscillations

For ripple analyses, we used EEG characteristics and the presence of multiple pyramidal cells to select tetrodes that were located in either the CA1 cell layer. We filtered the field potentials recorded from these tetrodes using a 30 tap 150 – 250 Hz bandpass FIR filter (100, 300 Hz stopband) designed using least squares with equal weighting across bands. The magnitude of this filtered signal was then extracted using the Hilbert transform. Ripples were detected using the criterion that the magnitude of the ripple-band field had to exceed its mean by a threshold of three standard deviations for at least 15 ms. Normalized ripple power was defined as standard deviations above this threshold(Cheng and Frank, 2008). Note that the ripple magnitude is a normalized measure and thus did not require further normalization to compare across animals. The magnitude for each ripple event was defined as the mean across tetrodes for which that event was detected. To look at the relationship between movement speed and ripple power, we computed the linear regression between the log of the mean speed during each ripple event and the normalized power of each event. For regression analyses we eliminated points with a speed below 1/8 cm/sec ensure robust linear fits in relation to log(speed). As the distribution of the residuals was non-Gaussian, we used a bootstrap resampling method to determine the significance of the linear regression. To investigate how the depth of modulation changed across exposures, we used a bootstrap estimate of slope for each exposure to ensure equal sampling across animals. To test for significant changes in slope over days, we used a permutation test to test against the null hypothesis. Briefly, we compared the correlation between exposure day and slope to the distribution of correlations obtained by permuting the identity of the exposure 1000

times before computing the correlation. To measure the within day differences in ripple power between novel and familiar experiences, we normalized all data to the familiar session. After binning the data into logarithmically spaced speed bins we used a rank sum test to measure the difference in normalized ripple power between comparable speeds in the novel and familiar track. To measure the within day differences in the depth of modulation between novel and familiar experience we computed 1000 bootstrap estimates of the slope to ensure equal sampling across animals and across different behaviors.

Residual Correlations

To determine whether speed altered the formation of cell assemblies, we computed the residual correlation between pairs of neurons with overlapping place fields. This approach, adapted from Singer et. al. (2010) examines the “noise” correlations, or how correlated trial to trial variability is among cell pairs. Residuals were calculated for each neuron as the difference between the expected number of spikes and the actual number of spikes recorded in 500ms bins. Spikes that occurred during ripples were excluded.

To determine the expected number of spikes we computed the expected firing rate in 33ms bins based on the animal's location in the track and the linearized place field. We then integrated that rate across each 500ms bin. We then calculated the residuals as the difference between the expected number of spikes and the actual number of spikes recorded in each time bin. We assigned each 500ms bin to one of four logarithmically spaced speed bins and computed the correlation between residuals of cell pairs for each speed bin. Correlations were only computed if there were at least 10 s of data to correlate, e.g., ≥20 bins in which both cells' expected firing rate was >0 Hz.

Bibliography

Alvarez P, Squire LR (1994) Memory consolidation and the medial temporal lobe: a simple network model. ProcNatlAcadSciUSA 91:7041-7045.

Amaral DG, Ishizuka N, Claiborne B (1990) Neurons, numbers and the hippocampal network. Prog Brain Res 83:1--11.

Amaral DG, Witter MP (1995) Hippocampal Formation. In: The Rat Nervous System, vol. Second (Paxinos, C., ed), pp 443-493: Academic Press.

Atallah BV, Scanziani M (2009) Instantaneous modulation of gamma oscillation frequency by balancing excitation with inhibition. Neuron 62:566-577.

Averbeck BB, Latham PE, Pouget A (2006) Neural correlations, population coding and computation. Nat Rev Neurosci 7:358-366.

Bartos M, Vida I, Jonas P (2007) Synaptic mechanisms of synchronized gamma oscillations in inhibitory interneuron networks. Nat Rev Neurosci 8:45-56.

Bliss TV, Lomo T (1973) Long-lasting potentiation of synaptic transmission in the dentate area of the anaesthetized rabbit following stimulation of the perforant path. JPhysiol 232:331-356.

Bokil H, Andrews P, Kulkarni JE, Mehta S, Mitra PP (2010) Chronux: a platform for analyzing neural signals. J Neurosci Methods 192:146-151.

Bragin A, Jando G, Nadasdy Z, Hetke J, Wise K, Buzsaki G (1995) Gamma (40-100 Hz) oscillation in the hippocampus of the behaving rat. Journal of Neuroscience 15:47-60.

Brun VH, Leutgeb S, Wu HQ, Schwarcz R, Witter MP, Moser EI, Moser MB (2008) Impaired Spatial Representation in CA1 after Lesion of Direct Input from Entorhinal Cortex. Neuron 57:290-302.

Buzsaki G (1986) Hippocampal sharp waves: their origin and significance. Brain Res 398:242-252.

Buzsaki G (1989) Two-stage model of memory trace formation: a role for "noisy" brain states. Neuroscience 31:551-570.

Buzsaki G (1996) The hippocampo-neocortical dialogue. CerebCortex 6:81-92.

Buzsaki G (2002) Theta oscillations in the hippocampus. Neuron 33:325-340.

Buzsaki G, Horvath Z, Urioste R, Hetke J, Wise K (1992) High-frequency network oscillation in the hippocampus. Science 256:1025-1027.

Buzsaki G, Leung LW, Vanderwolf CH (1983) Cellular bases of hippocampal EEG in the behaving rat. Brain Res 287:139-171.

Cardin JA, Carlen M, Meletis K, Knoblich U, Zhang F, Deisseroth K, Tsai LH, Moore CI (2009) Driving fast-spiking cells induces gamma rhythm and controls sensory responses. Nature 459:663-667.

Carr MF, Jadhav SP, Frank LM (2011) Hippocampal replay in the awake state: a potential substrate for memory consolidation and retrieval. NatNeurosci 14:147-153.

Chen Z, Resnik E, McFarland JM, Sakmann B, Mehta MR (2011) Speed controls the amplitude and timing of the hippocampal gamma rhythm. PLoS One 6:e21408.

Cheng S, Frank LM (2008) New experiences enhance coordinated neural activity in the hippocampus. Neuron 57:303-313.

Chevaleyre V, Siegelbaum SA (2010) Strong CA2 pyramidal neuron synapses define a powerful disynaptic cortico-hippocampal loop. Neuron 66:560-572.

Chrobak JJ, Buzsaki G (1994) Selective activation of deep layer (V-VI) retrohippocampal cortical neurons during hippocampal sharp waves in the behaving rat. Journal of Neuroscience 14:6160-6170.

Chrobak JJ, Buzsaki G (1996) High-frequency oscillations in the output networks of the hippocampal- entorhinal axis of the freely behaving rat. Journal of Neuroscience 16:3056-3066.

Chrobak JJ, Buzsaki G (1998) Gamma oscillations in the entorhinal cortex of the freely behaving rat. Journal of Neuroscience 18:388-398.

Cohen NJ, Eichenbaum H (1993) Memory, Amnesia, and the Hippocampal System. Cambridge, MA: M.I.T. Press.

Colgin LL, Denninger T, Fyhn M, Hafting T, Bonnevie T, Jensen O, Moser MB, Moser EI (2009) Frequency of gamma oscillations routes flow of information in the hippocampus. Nature %19;462:353-357.

Csicsvari J, Hirase H, Czurko A, Mamiya A, Buzsaki G (1999) Fast Network Oscillations in the Hippocampal CA1 Region of the Behaving Rat. Journal of Neuroscience 19:RC20.

Csicsvari J, Hirase H, Mamiya A, Buzsaki G (2000) Ensemble patterns of hippocampal CA3-CA1 neurons during sharp wave-associated population events. Neuron 28:585-594.

Csicsvari J, Jamieson B, Wise KD, Buzsaki G (2003) Mechanisms of gamma oscillations in the hippocampus of the behaving rat. Neuron 37:311-322.

Csicsvari J, O'Neill J, Allen K, Senior T (2007) Place-selective firing contributes to the reverse-order reactivation of CA1 pyramidal cells during sharp waves in open-field exploration. EurJNeurosci 26:704-716.

Davidson TJ, Kloosterman F, Wilson MA (2009) Hippocampal replay of extended experience. Neuron 63:497-507.

Diba K, Buzsaki G (2007) Forward and reverse hippocampal place-cell sequences during ripples. NatNeurosci 10:1241-1242.

Diekelmann S, Born J (2010) Slow-wave sleep takes the leading role in memory reorganization. NatRevNeurosci 11:218.

Dragoi G, Buzsaki G (2006) Temporal encoding of place sequences by hippocampal cell assemblies. Neuron 50:145-157.

Dudai Y (2004) The neurobiology of consolidations, or, how stable is the engram? AnnuRevPsychol 55:51-86.:51-86.

Dupret D, O'Neill J, Pleydell-Bouverie B, Csicsvari J (2010a) The reorganization and reactivation of hippocampal maps predict spatial memory performance. Nat Neurosci 13:995-1002.

Dupret D, O'Neill J, Pleydell-Bouverie B, Csicsvari J (2010b) The reorganization and reactivation of hippocampal maps predict spatial memory performance. NatNeurosci 13:995-1002.

Ego-Stengel V, Wilson MA (2010) Disruption of ripple-associated hippocampal activity during rest impairs spatial learning in the rat. Hippocampus 20:1-10.

Eichenbaum H, Cohen NJ (2001) From Conditioning to Conscious Recollection. New York: Oxford University Press.

Epsztein J, Brecht M, Lee AK (2011) Intracellular determinants of hippocampal CA1 place and silent cell activity in a novel environment. Neuron 70:109-120.

Fell J, Axmacher N (2011) The role of phase synchronization in memory processes. Nat Rev Neurosci 12:105-118.

Fell J, Klaver P, Elfadil H, Schaller C, Elger CE, Fernandez G (2003) Rhinal-hippocampal theta coherence during declarative memory formation: interaction with gamma synchronization? Eur J Neurosci 17:1082-1088.

Foster DJ, Wilson MA (2006) Reverse replay of behavioural sequences in hippocampal place cells during the awake state. Nature 440:680-683.

Fox SE, Ranck JB, Jr. (1981) Electrophysiological characteristics of hippocampal complex-spike cells and theta cells. ExpBrain Res 41:399-410.

Frank LM, Brown EN, Wilson MA (2000) Trajectory encoding in the hippocampus and entorhinal cortex. Neuron 27:169-178.

Frank LM, Brown EN, Wilson MA (2001) A Comparison of the Firing Properties of Putative Excitatory and Inhibitory Neurons From CA1 and the Entorhinal Cortex. Journal of Neurophysiology 86:2029-2040.

Frank LM, Stanley GB, Brown EN (2004) Hippocampal plasticity across multiple days of exposure to novel environments. Journal of Neuroscience 24:7681-7689.

Freund TF, Buzsaki G (1996) Interneurons of the hippocampus. Hippocampus 6:347-470.

Giovannini MG, Rakovska A, Benton RS, Pazzagli M, Bianchi L, Pepeu G (2001) Effects of novelty and habituation on acetylcholine, GABA, and glutamate release from the frontal cortex and hippocampus of freely moving rats. Neuroscience 106:43-53.

Girardeau G, Benchenane K, Wiener SI, Buzsaki G, Zugaro MB (2009) Selective suppression of hippocampal ripples impairs spatial memory. NatNeurosci 12:1222-1223.

Harris KD, Csicsvari J, Hirase H, Dragoi G, Buzsaki G (2003) Organization of cell assemblies in the hippocampus. Nature 424:552-556.

Hasselmo ME (1999) Neuromodulation: acetylcholine and memory consolidation. Trends Cogn Sci 3:351-359.

Hasselmo ME, Schnell E (1994) Laminar selectivity of the cholinergic suppression of synaptic transmission in rat hippocampal region CA1: computational modeling and brain slice physiology. Journal of Neuroscience 14:3898-3914.

Hebb DO (1949) The organization of behavior. New York, NY: Wiley.

Hen I, Sakov A, Kafkafi N, Golani I, Benjamini Y (2004) The dynamics of spatial behavior: how can robust smoothing techniques help? JNeurosciMethods 133:161-172.

Jarrard LE (2001) Retrograde amnesia and consolidation: anatomical and lesion considerations. Hippocampus 11:43-49.

Jensen O, Lisman JE (1996) Theta/gamma networks with slow NMDA channels learn sequences and encode episodic memory: role of NMDA channels in recall. LearnMem 3:264-278.

Johnson A, Redish AD (2007) Neural ensembles in CA3 transiently encode paths forward of the animal at a decision point. Journal of Neuroscience 27:12176-12189.

Jutras MJ, Fries P, Buffalo EA (2009) Gamma-band synchronization in the macaque hippocampus and memory formation. Journal of Neuroscience 29:12521-12531.

Karlsson MP, Frank LM (2008) Network Dynamics Underlying the Formation of Sparse, Informative Representations in the Hippocampus. Journal of Neuroscience 28:14271-14281.

Karlsson MP, Frank LM (2009) Awake replay of remote experiences in the hippocampus. NatNeurosci 12:913-918.

Kelemen E, Fenton AA (2010) Dynamic grouping of hippocampal neural activity during cognitive control of two spatial frames. PLoSBiol 8:e1000403.

Kim JJ, Fanselow MS (1992) Modality-specific retrograde amnesia of fear. Science 256:675-677.

Kim SM, Frank LM (2009) Hippocampal lesions impair rapid learning of a continuous spatial alternation task. PLoSONE 4:e5494.

King C, Recce M, O'Keefe J (1998) The rhythmicity of cells of the medial septum/diagonal band of Broca in the awake freely moving rat: relationships with behaviour and hippocampal theta. EurJNeurosci 10:464-477.

Klausberger T, Magill PJ, Marton LF, Roberts JD, Cobden PM, Buzsaki G, Somogyi P (2003) Brain-state- and cell-type-specific firing of hippocampal interneurons in vivo. Nature %20;421:844-848.

Kopell N, Ermentrout GB, Whittington MA, Traub RD (2000) Gamma rhythms and beta rhythms have different synchronization properties. Proc Natl Acad Sci U S A 97:1867--1872.

Kudrimoti HS, Barnes CA, McNaughton BL (1999) Reactivation of hippocampal cell assemblies: effects of behavioral state, experience, and EEG dynamics. Journal of Neuroscience 19:4090-4101.

Lee AK, Wilson MA (2002) Memory of sequential experience in the hippocampus during slow wave sleep. Neuron 36:1183-1194.

Lee MG, Chrobak JJ, Sik A, Wiley RG, Buzsaki G (1994) Hippocampal theta activity following selective lesion of the septal cholinergic system. Neuroscience 62:1033-1047.

Leung LS (1980) Behavior-dependent evoked potentials in the hippocampal CA1 region of the rat. I. Correlation with behavior and EEG. Brain Res 198:95-117.

Lever C, Burton S, O'Keefe J (2006) Rearing on hind legs, environmental novelty, and the hippocampal formation. RevNeurosci 17:111-133.

Lisman JE, Otmakhova NA (2001) Storage, recall, and novelty detection of sequences by the hippocampus: elaborating on the SOCRATIC model to account for normal and aberrant effects of dopamine. Hippocampus 11:551-568.

Marr D (1971) Simple memory: a theory for archicortex. PhilosTransRSocLond 262:23-81.

McNaughton BL, Morris RG (1987) Hippocampal synaptic enhancement and information storage within a distributed memory system. Trends in Neurosciences 10:408-415.

Memmesheimer RM (2010) Quantitative prediction of intermittent high-frequency oscillations in neural networks with supralinear dendritic interactions. Proc Natl Acad Sci U S A 107:11092-11097.

Mizuseki K, Sirota A, Pastalkova E, Buzsaki G (2009) Theta oscillations provide temporal windows for local circuit computation in the entorhinal-hippocampal loop. Neuron 64:267-280.

Montgomery SM, Betancur MI, Buzsaki G (2009) Behavior-dependent coordination of multiple theta dipoles in the hippocampus. Journal of Neuroscience 29:1381-1394.

Montgomery SM, Buzsaki G (2007) Gamma oscillations dynamically couple hippocampal CA3 and CA1 regions during memory task performance. Proc Natl Acad Sci U S A 104:14495-14500.

Montgomery SM, Sirota A, Buzsaki G (2008) Theta and gamma coordination of hippocampal networks during waking and rapid eye movement sleep. J Neurosci 28:6731-6741.

Moser E, Mathiesen I, Andersen P (1993) Association between brain temperature and dentate field potentials in exploring and swimming rats. Science 259:1324--1326.

Murray AJ, Sauer JF, Riedel G, McClure C, Ansel L, Cheyne L, Bartos M, Wisden W, Wulff P (2011) Parvalbumin-positive CA1 interneurons are required for spatial working but not for reference memory. Nat Neurosci 14:297-299.

Nadel L, Moscovitch M (2001) The hippocampal complex and long-term memory revisited. Trends Cogn Sci 5:228--230.

Nakashiba T, Buhl DL, McHugh TJ, Tonegawa S (2009) Hippocampal CA3 output is crucial for ripple-associated reactivation and consolidation of memory. Neuron 62:781-787.

Nakashiba T, Young JZ, McHugh TJ, Buhl DL, Tonegawa S (2008) Transgenic inhibition of synaptic transmission reveals role of CA3 output in hippocampal learning. Science 319:1260-1264.

Nitz D, McNaughton B (2004) Differential modulation of CA1 and dentate gyrus interneurons during exploration of novel environments. JNeurophysiol 91:863-872.

O'Keefe J, Dostrovsky J (1971) The hippocampus as a spatial map. Preliminary evidence from unit activity in the freely-moving rat. Brain Res 34:171-175.

O'Keefe J, Nadel L (1978) The hippocampus as a cognitive map. London: Oxford University Press.

O'Neill J, Pleydell-Bouverie B, Dupret D, Csicsvari J (2010) Play it again: reactivation of waking experience and memory. Trends Neurosci 33:220-229.

O'Neill J, Senior T, Csicsvari J (2006) Place-selective firing of CA1 pyramidal cells during sharp wave/ripple network patterns in exploratory behavior. Neuron 49:143-155.

O'Neill J, Senior TJ, Allen K, Huxter JR, Csicsvari J (2008) Reactivation of experience-dependent cell assembly patterns in the hippocampus. NatNeurosci 11:209-215.

Osipova D, Takashima A, Oostenveld R, Fernandez G, Maris E, Jensen O (2006) Theta and gamma oscillations predict encoding and retrieval of declarative memory. J Neurosci 26:7523-7531.

Parikh V, Kozak R, Martinez V, Sarter M (2007) Prefrontal acetylcholine release controls cue detection on multiple timescales. Neuron 56:141-154.

Percival DB, Walden AT (1993) Spectral analysis for physical applications : multitaper and conventional univariate techniques. Cambridge ; New York, NY, USA: Cambridge University Press.

Ranck JB, Jr. (1973) Studies on single neurons in dorsal hippocampal formation and septum in unrestrained rats. I. Behavioral correlates and firing repertoires. ExpNeurol 41:461-531.

Rivas J, Gaztelu JM, Garcia-Austt E (1996) Changes in hippocampal cell discharge patterns and theta rhythm spectral properties as a function of walking velocity in the guinea pig. ExpBrain Res 108:113-118.

Rudy JW, Sutherland RJ (1995) Configural association theory and the hippocampal formation: an appraisal and reconfiguration. Hippocampus 5:375-389.

Segal M (1978) A correlation between hippocampal responses to interhemispheric stimulation, hippocampal slow rhythmic activity and behaviour. ElectroencephalogrClinNeurophysiol 45:409-411.

Siapas AG, Wilson MA (1998) Coordinated interactions between hippocampal ripples and cortical spindles during slow-wave sleep. Neuron 21:1123-1128.

Singer AC, Karlsson MP, Nathe AR, Carr MF, Frank LM (2010) Experience-dependent development of coordinated hippocampal spatial activity representing the similarity of related locations. Journal of Neuroscience 30:11586-11604.

Sohal VS, Zhang F, Yizhar O, Deisseroth K (2009) Parvalbumin neurons and gamma rhythms enhance cortical circuit performance. Nature 459:698-702.

Squire LR (1982) The neuropsychology of human memory. AnnuRevNeurosci 5:241-73:241-273.

Squire LR (1992) Memory and the hippocampus: a synthesis from findings with rats, monkeys, and humans [published erratum appears in Psychol Rev 1992 Jul;99(3):582]. PsycholRev 99:195-231.

Squire LR, Zola-Morgan S (1991) The medial temporal lobe memory system. Science 253:1380-1386.

Sullivan D, Csicsvari J, Mizuseki K, Montgomery S, Diba K, Buzsaki G (2011) Relationships between Hippocampal Sharp Waves, Ripples, and Fast Gamma Oscillation: Influence of Dentate and Entorhinal Cortical Activity. J Neurosci 31:8605-8616.

Taxidis J, Coombes S, Mason R, Owen MR (2011) Modeling sharp wave-ripple complexes through a CA3-CA1 network model with chemical synapses. Hippocampus.

Tort AB, Komorowski RW, Manns JR, Kopell NJ, Eichenbaum H (2009) Theta-gamma coupling increases during the learning of item-context associations. Proc Natl Acad Sci U S A 106:20942-20947.

Traub RD, Bibbig A (2000) A model of high-frequency ripples in the hippocampus based on synaptic coupling plus axon-axon gap junctions between pyramidal neurons. J Neurosci 20:2086--2093.

Tukker JJ, Fuentealba P, Hartwich K, Somogyi P, Klausberger T (2007) Cell type-specific tuning of hippocampal interneuron firing during gamma oscillations in vivo. J Neurosci 27:8184-8189.

Whishaw IQ, Vanderwolf CH (1973) Hippocampal EEG and behavior: changes in amplitude and frequency of RSA (theta rhythm) associated with spontaneous and learned movement patterns in rats and cats. BehavBiol 8:461-484.

Whitlock JR, Heynen AJ, Shuler MG, Bear MF (2006) Learning Induces Long-Term Potentiation in the Hippocampus. Science 313:1093-1097.

Wierzynski CM, Lubenov EV, Gu M, Siapas AG (2009) State-dependent spike-timing relationships between hippocampal and prefrontal circuits during sleep. Neuron 61:587-596.

Wilson MA, McNaughton BL (1993) Dynamics of the hippocampal ensemble code for space. Science 261:1055-1058.

Wilson MA, McNaughton BL (1994) Reactivation of hippocampal ensemble memories during sleep. Science 265:676-679.

Winson J, Abzug C (1978) Neuronal transmission through hippocampal pathways dependent on behavior. JNeurophysiol 41:716-732.

Womelsdorf T, Schoffelen JM, Oostenveld R, Singer W, Desimone R, Engel AK, Fries P (2007) Modulation of neuronal interactions through neuronal synchronization. Science 316:1609-1612.

Ylinen A, Bragin A, Nadasdy Z, Jando G, Szabo I, Sik A, Buzsaki G (1995) Sharp wave-associated high-frequency oscillation (200 Hz) in the intact hippocampus: network and intracellular mechanisms. Journal of Neuroscience 15:30-46.

Publishing Agreement

It is the policy of the University to encourage the distribution of all theses, dissertations, and manuscripts. Copies of all UCSF theses, dissertations, and manuscripts will be routed to the library via the Graduate Division. The library will make all theses, dissertations, and manuscripts accessible to the public and will preserve these to the best of their abilities, in perpetuity.

I hereby grant permission to the Graduate Division of the University of California, San Francisco to release copies of my thesis, dissertation, or manuscript to the Campus Library to provide access and preservation, in whole or in part, in perpetuity.

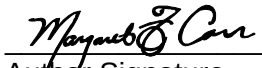

Author Signature

8/15/2011

Date